2019-01-01

Development Of Actuators Using Material Extrusion Additive Manufacturing With Embedded Shape Memory Alloy Wire

Alfonso Fernandez
University of Texas at El Paso, ponchito.defjam@gmail.com

DEVELOPMENT OF ACTUATORS USING MATERIAL EXTRUSION ADDITIVE MANUFACTURING WITH EMBEDDED SHAPE MEMORY ALLOY WIRE

ALFONSO FERNANDEZ

Master's Program in Mechanical Engineering

APPROVED:

Ryan R. Wicker, Ph.D., Chair

David Espalin, Ph.D.

Amit Lopes, Ph.D.

Charles Ambler, Ph.D.
Dean of the Graduate School

This thesis is dedicated to God as I am doing this for him and not for me.

DEVELOPMENT OF ACTUATORS USING MATERIAL EXTRUSION ADDITIVE MANUFACTURING WITH EMBEDDED SHAPE MEMORY ALLOY WIRE

by

ALFONSO FERNANDEZ, B.S.M.E.

Thesis

Presented to the Faculty of the Graduate School of

The University of Texas at El Paso

in Partial Fulfillment

of the Requirements

for the Degree of

MASTER OF SCIENCE

Department of Mechanical Engineering

THE UNIVERSITY OF TEXAS AT EL PASO

May 2019

ACKNOWLEDGEMENTS

I am very grateful to Dr. David Espalin as he has been an immense role model for my career and person. The values he has shown me as a researcher have induced in me a very strong foundation to become a very successful researcher. Dr. Ryan Wicker, director of the W.M. Keck Center for 3D Innovation, for he has been always helpful and his guidance invaluable. This thesis work would have not been possible if not for the great facility that Dr. Wicker has constructed.

I would also like to thank Mr. Jose Motta for he has always been with me in this research helping with all the experiments and literature review. Dr. Hilmar Koerner for his exigent demands that made this thesis what it is.

Finally, I would like to thank my family for they have never ceased to push me forward into finishing this work. In particular, I would like to acknowledge the memory of my dad Alfonso, which has inspired me to follow my dreams and to continue to become better for myself and everyone that surrounds me.

ABSTRACT

Over the past several decades, the advancements in Additive Manufacturing (AM) technologies have opened a wide variety of applications where AM can be used. Some examples of these advancements are the introduction of automatic wire embedding capabilities, the introduction of multi-material processing and the printing of thermoplastic elastomers. With the availability of these advancements, it is now possible to create spark-free, dust-free actuation mechanisms for applications where it is crucial that no spark is generated (i.e. space shuttle fuel valve).

In this research, a Lulzbot TAZ 6 desktop material extrusion system was utilized to print parts out of Plasticized Copolymer Thermoplastic Elastomer (PCTPE) with manually embedded Flexinol shape memory alloy (SMA) wire to create 3D printed movable parts that could be used for actuation in larger systems. The part's motion relies upon the activation of the SMA and on the recovery of the initial shape by the polymer's stiffness, when the wire ceases to be activated. This activation was achieved by joule heating, where the current input was calculated using a heat transfer mathematical model. The design was driven by dimensions obtained through bending stress calculations that modeled the force exerted by the activated wire on the polymer surrounding the wire. The design based on the calculations was fabricated and reproduced a motion of ~1.8 mm. It is concluded that actuators are possible to be created using AM with the embedding of SMA wires; however, the design for fabrication can be very limited.

TABLE OF CONTENTS

LIST OF FIGURES

LIST OF TABLES

CHAPTER 1: INTRODUCTION

1.1 BACKGROUND

Additive Manufacturing (AM) is the process by which a computerized three-dimensional model is manufactured through a process that adds material in a layer-by-layer basis (Bourell *et al.*, 2014). This means that parts are created through stacking layers of material having the shape of the cross-sectional area at the precise height of the layer being constructed. This layer by layer manufacturing technique presents new opportunities in the design of freeform structures beyond what conventional manufacturing processes can provide.

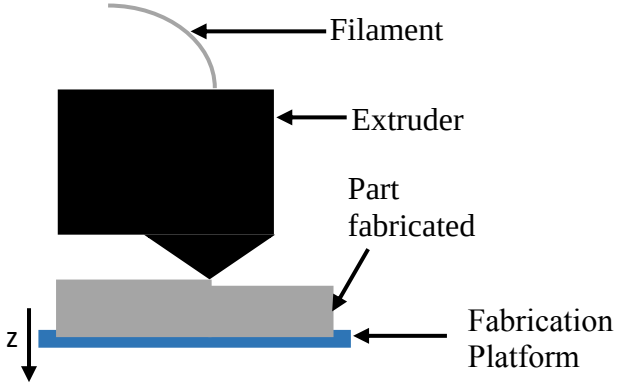

Figure 1: Material extrusion schematic in an x-z plane

Material extrusion is a type of AM technology that consists of the deposition of semi-molten thermoplastic material through a heated nozzle that moves in an x-y plane. After the nozzle has covered the entire cross-sectional area of the layer, either the stage or the extruder moves in the z direction for the addition of another layer on top of the previously built layer, continuing the building process (Figure 2). This construction is done by the nozzle (typically between 0.127mm and 1.2mm in diameter) rapidly, between 10 mm/sec and 200 mm/sec, depending on the material being extruded.

Initially, the AM technology was only used for Rapid Prototyping as a way of physically creating ideas (Wong and Hernandez, 2012) at a low cost, compared to a traditional manufacturing technique, within days or even hours of designing (Cooper, 2005). The mechanical properties and the dimensional accuracy of the AM technologies have been improved in such a way that AM is not used only for rapid prototyping anymore; AM is now being used to create functional end-use parts. The research conducted in material extrusion AM (Ambriz *et al.*, 2017) has made the technology usable to create multifunctional components (MacDonald *et al.*, 2014). The addition

of multiple technologies such as wire embedding has improved this technology for the creation of electrically functional parts (Shemelya *et al.*, 2015, Espalin *et al.*, 2014), multifunctional satellite structures (Shemelya *et al.*, 2015) and other structures for antenna fabrication (MacDonald *et al.*, 2018, Shemelya *et al.*, 2015). These significant advancements enable the technology to be used for a wide variety of applications.

1.2 MOTIVATION

It is possible to combine material extrusion AM with other technologies through the interruption of the manufacturing process. When this interruption happens, other manufacturing technologies can be used to act on the part under fabrication to create multi-material and multi-functional parts. In this particular case, wire-embedding and electronic component placement technologies were used to introduce electrical components and wire into parts (see Ambriz *et al.*, 2017 for more details on the hybrid manufacturing system and setup). By incorporating multiple technologies together, many new enhanced applications of manufactured objects are enabled by providing capabilities for fabricating end-use freeform objects with multiple functionalities. Although several electrically functional parts have been created and tested previously (Shemelya *et al.*, 2015), the present research represents an attempt at including motion (actuation) as part of the enhanced functionalities. The availability of thermoplastic elastomers and Shape Memory Alloy (SMA) wire enables the present material extrusion technology to print movable parts. This can be accomplished with the material extrusion of thermoplastic elastomers and the embedding of SMA wires in structures and patterns that are designed for specific motion. Therefore, the main motivation of this research is to develop a methodology for embedding SMA wire into flexible thermoplastic parts created through material extrusion AM for further implementation with an automatic thermal wire embedder integrated in a hybrid AM setup. The developed methodology will enable the creation of spark-free, dust-free actuators and sensors through an automated AM process that could eventually be used for aerospace applications.

1.3 THESIS OBJECTIVES

This thesis includes several objectives that are listed below.

1. Determine the driving mechanism of the actuator
2. Determine the properties desired for polymer selection
3. Develop numerical method to calculate the current required for activation of SMA
4. Develop a numerical method to determine the dimensional constraints to be used in the design process
5. Analyze the current/time graphs to validate the temperature mathematical model
6. Fabricate and test actuator with calculated dimensions and current input

1.4 THESIS OUTLINE

The research in this thesis is presented in a total of six chapters. Chapter 1 provided an introduction and motivation for the research. Chapter 2 includes a literature review regarding relevant subjects for this study. In Chapter 3, an overview of the concept of 3D printed actuators, the material selection and the mathematical models are provided. Chapter 4 describes the experimental setup for determining the adhesion strength, the mathematical model validation tests, and the repeatability tests performed to determine the behavior of the actuator under periodic activation. The results for these experiments are presented and discussed in Chapter 5. Finally, the conclusions and future work recommendations are included in Chapter 6.

CHAPTER 2: LITERATURE REVIEW

2.1 INTRODUCTION

Additive manufacturing (AM) technology refers to a layer-by-layer manufacturing process. This technique was used for the construction of prototypes initially, and its recent advancements have made this technology available for more sophisticated applications such as biomedical implants and structures with embedded sensors and electronics (Shemelya *et al.*, 2016). The AM process takes a Computer Aided Design (CAD) file and makes a 3D modeled part through the different AM processes that are available. The application determines which technology and which material is to be used for manufacturing, and the options include plastics, metals, ceramics and composites with the material to be processed in liquid, particle, filament, wire, and other forms. Each option of material uses a unique technology to process it; some of the processing techniques use lasers, electron beams or extruders.

AM has an overall set of steps that apply for all technologies. Following is a protocol describing these steps:

1. First, a CAD model must be generated and converted to STL format.
2. The STL file must be processed by machine specific software to generate the toolpath commands that control the particular AM system used to manufacture the part.
3. The system must be set up according to the specific technology
4. Part fabrication start
5. The part typically requires post processing that also depends on the specific AM technology used for manufacturing.

The layer by layer process that AM uses oftentimes results in defects such as porosity in the final parts, and these layer by layer defects reduce the overall mechanical properties of the parts. Also, the nature of this process results in parts with high surface roughness compared to that of traditional machining. Methods for improving these limitations have been explored by

researchers for many years introducing post processing of the parts such as heat treatments (Frazier, 2014), surface machining techniques (Saunders, 2017) and parameter optimization (Hossain *et al*., 2014). Other issues impacting the adoption of AM include the high costs of materials used in the process, the slow production of parts (relative to production technologies such as plastic injection molding), and the large variability of mechanical properties from part to part (Grace, 2016). Some reduction in material costs have resulted from the increase of material providers (Wohlers report, 2018). The slow production and the high variability of mechanical properties has been tackled with higher quality machines and more control over variables that affect the build.

2.2 MATERIAL EXTRUSION

Material extrusion is a technology that fabricates components using a nozzle, typically ranging between 0.127mm and 1.2mm, that extrudes material on an x-y gantry that, in a layer-by-layer basis, completes the cross-sectional shape of the structure to be printed (ASTM F2792, 2012). This technology was developed by Stratasys Inc. under the name of Fused Deposition Modeling (FDM) and commercialized in 1990. After a fundamental FDM patent expired, several open-source machines started to enter the market (Wohlers Report, 2018). After that, in 2012 the ASTM International published a standard terminology for additive manufacturing technologies where Material Extrusion was defined to refer to the FDM technology.

Material extrusion follows the same protocol for all AM processes presented before in section 2.1 with slight variations that are specific to the technology (Singh, R., 2010):

1. Generation of STL model from CAD
2. Processing of STL in slicing software for layer and toolpath creation
    a. Selection of material
    b. Selection of parameters specific to material and quality of build
3. File import to material extrusion machine
4. Machine preparation

c. Filament of material introduced to extruder

d. Build platform prepared with suitable build sheet

5. Build part
6. Removal of part from build sheet
7. Removal of support created to aid build

For a successful build, there are parameters that must be selected for a specific material. These typical build parameters include: extruder temperature, platform temperature, layer thickness, material flow and raster width. These processing parameters are critical because each plays an important role in how the manufacturing takes place. If the temperature is not high enough (above glass transition temperature, for example), the extruder will not deposit material. On the other hand, if the temperature is too high, the filament will burn in the extruder. The platform temperature must be increased to enhance the adhesion of the part to the platform, otherwise it will not stick, and printing will be unsuccessful. The layer thickness and road width determine what flow rate of material will be needed to have a quality print. If these three parameters are not calibrated to each other, the extruded material will either be excessive or not be enough and the final part will suffer in dimensional accuracy and surface finish, among other things. A Lulzbot TAZ 5 was the material extrusion desktop system selected for this study. It fabricates using a thermoplastic filament of 3mm and a nozzle size of 0.6mm. The slicing software allows for parameter development such as road width size, thickness, temperatures among others.

This technology holds several issues related to porosity, interlayer bonding, dimensional accuracy and surface roughness. However, these issues can be improved. Porosity can be reduced by modifying the raster to raster distance and the flow of material through the nozzle. As a result of porosity reduction, interlayer bonding can also be increased. Dimensional accuracy and surface roughness have been improved by using thinner nozzles with diameters of 0.127mm and by reducing the layer thickness (Espalin *et al.*, 2014). Other post-processing has been performed on the surface of parts to increase part accuracy and surface roughness such as machining of the previously manufactured layer. Over the past few years, researchers have dedicated to find new

and more advanced applications for this technology such as the creation of electro-mechanical systems with the embedding of wires in the process (Aguilera *et al.*, 2013) and the manufacturing of electrically functional structures (Shemelya *et al*., 2015). The technology, through the recent research-enabled advancements, has broadened the applications in which it can be used. Now it is possible to make not only complex structures for prototypes, but also functional electrical parts by introducing electronics, copper wires and foil, while interrupting the building procedure (Coronel *et al.*, 2017). With thermoplastic elastomers being available for extrusion, it is possible now to produce parts with integrated motion capabilities by embedding SMA wire into the manufactured parts.

2.3 FLEXIBLE THERMOPLASTIC POLYMERS

In additive manufacturing, several materials can be used for fabrication of components. The material selected for fabrication is always dependent on the application where the component is going to be used and the technology where it will be manufactured. For material extrusion, the selection of material is in the range of thermoplastic polymers. Thermoplastic polymers are materials composed of many monomer chains, joined together through electrical bonds. These bonds are called van der Waals forces. It is through these weak forces that polymers soften when their temperature is increased past a determined temperature where these bonds are broken. This temperature is called glass transition temperature (T_g) and is where the polymer material starts to soften without modifying the chemical structure of the polymer. This allows for modifying the shape of the material when heated. Material extrusion AM takes advantage of this property of thermoplastics for manufacturing. Thermosets are another class of polymer materials. While thermoplastics can be molded every time they are heated up past their glass transition temperature, thermosets go through chemical changes when treated with temperature or chemicals. This chemical change connects the molecule chains, forming a single macromolecule. The connections formed by this chemical change are commonly known as crosslinks. Some of these thermoplastics are used for rapid prototyping and modeling, such as Acrylonitrile Butadiene Styrene (ABS),

Polylactic Acid (PLA), and nylon. Other materials that are stronger are used for structural components such as Polycarbonate and ULTEM. These materials are recognized for having a semi-crystalline molecular structure or an amorphous molecular structure. The amorphous molecular structure refers to a random structure where the polymer chains are not ordered in a specific direction. This random structure makes the polymer have a temperature range where it gradually softens until reaching full melting. In contrast, the semi-crystalline polymers have an ordered structure of the polymer chains where most chains are accommodated to the same direction. This semi-crystalline structure makes the polymer have a more defined melting temperature, meaning that the polymers with this type of structure go through a smaller softening range than amorphous polymers.

Some applications call for other kinds of materials such as flexible thermoplastics (with modulus ranging from 12 MPa to 75 MPa) that are used for components that are required to deform and recover to the printed shape. There is not a very wide range of flexible materials for printing, because the applications they can be used in are limited due to their mechanical properties. The thermoplastic polymers that are used currently for AM are the Thermoplastic Elastomers (TPEs), because they are materials that possess a combination of properties from semi-crystalline materials and from soft elastomers (Spontak and Patel, 2000). Basically, they have two phases where the stiff segments are connected to flexible segments. This connection provides mechanical properties that are thermally reversible which is an ideal feature for extruding mechanisms of manufacturing (Feng *et al*., 2017) because it allows for the heated material to be formed into the desired shape. In this group of thermoplastics there is a broad variety of materials that can be used. Table 1 contains the most common materials for 3D printing with their glass transition temperature and Young's Modulus.

Table 2: Some of the common thermoplastics available for 3D printing with their respective glass transition temperature and Young's Modulus

Thermoplastic	Glass-Transition Temperature (°C)	Modulus (MPa)
ABS	105	2500
PC	147	2600
ULTEM	215	3040
PLA	60	3500
Nylon 6	47	2000
Polypropylene	-10	1500
HIPS	100	1900
PET	72	2700
ASA	100	2600
PVA	80	5100
Ninjaflex TPU	-35	12
PCTPE	76	75
ABS10:SEBS90	-65	15

Thermoplastic Polyurethanes (TPUs) are thermoplastic elastomers that possess a complex morphology due to the hard and soft segment blocks being not entirely separated from each other. The presence of hard segments in the soft regions of the polymer blocks increase the glass transition temperature of the soft microphase of the thermoplastic, as well as the presence of soft segments in the hard regions would decrease the glass transition temperature of the hard regions (Eceiza *et al*., 2012). Figure 2 shows a schematic of the polymer chains for a thermoplastic and

Figure 2: Thermoplastic and thermoplastic elastomer polymer chain schematic

for a thermoplastic elastomer. The Ninjaflex TPU, which is a material provided by the Fenner Drives company was selected for this study due to its low modulus of 12 MPa.

Another TPE that was used for this study is a blend of SEBS and ABS developed by Dr. David Roberson (Siqueiros *et al*., 2016). This polymer is composed of 90% by weight of Styrene-Ethylene-Butylene-Styrene (SEBS) and 10% by weight of Acrylonitrile-Butadiene-Styrene (ABS). The high percentage of SEBS creates the softness of the polymer which lets the blend have a 15 MPa modulus, in comparison with the 12 MPa modulus of the TPU previously described. Although this polymer has a higher modulus than the TPU, the adhesion properties that it exhibits over the TPU are studied in this project to determine what polymer was to be used.

Another flexible polymer that was used for this project is the Plasticized Copolyamide Thermoplastic Elastomer (PCTPE). It is a blend of a type of low-modulus nylon and a thermoplastic elastomer that are not specified by the manufacturer. The final manufacturing stage of this filament material is stretching the material to increase the tensile properties of the filament. This is to prevent buckling on the extruder; problem that many other flexible polymers exhibit. This means that after extruding, the polymer tends to be more flexible than in filament form. This material has a modulus of 75 MPa which is about five times that of the ABS/SEBS blend and the TPU which are 15 MPa and 12 MPa, respectively. This means that the PCTPE is less flexible than the ABS/SEBS blend and the TPU. However, the glass transition temperature of the ABS/SEBS blend is -65°C and that of the TPU is -35°C which is much lower than that of the PCTPE which is about 76°C. The comparison that Table 1 offers helps in the decision of material to be used for the polymer part. The criteria for selecting is to have a modulus that would allow for the activation force of the wire to move the part and to have a T_g lower than the activation temperature of the wire.

2.4 WIRE EMBEDDING

Wire embedding is a technology developed in the W.M. Keck Center for 3D Innovation in the University of Texas at El Paso for introducing wires into additively manufactured components.

These technologies were developed as an improvement for interconnects in additively manufactured structural electronics that were developed with conductive inks. Conductive inks possess high resistivity (30-35μΩ-cm) in comparison with solid copper wire (1.68 μΩ-cm). For this reason, it was decided to change the interconnect technology to directly embed solid copper wire.

Several methods were explored for wire embedding such as ultrasonic, Joule and thermal embedding. Each method represents a different challenge and a different approach. All methods involve the feed of wire through an embedding tool and laying it down over an additively manufactured surface. The technology has been explored to an extent where a wire embedding tool has already been integrated into several AM technologies, including a desktop system.

The process can be described in several steps: (1) Additive manufacturing of component until layer where embedding will occur; (2) deployment of wire embedding tool; (3) wire embedding; (4) retraction of wire embedding tool; (5) resume of fabrication. This process is not dependent on the method of embedding, all methods accommodate these steps.

The first method explored for wire embedding was ultrasonic embedding. This method consists of the use of an ultrasonic horn with a wire fed through the center of the probe to embed the wire perpendicularly on the substrate as shown in Figure 3. The ultrasonic horn moves up and down at ultrasonic frequencies (15-40kHz), locally heating up the wire while it is dragged across the 3D printed surface to create the trace intended. This local heating is desired since heating up more of the wire could result in several issues that will be described below. The parameter that can be changed to achieve optimal embedding is the amplitude of motion of the

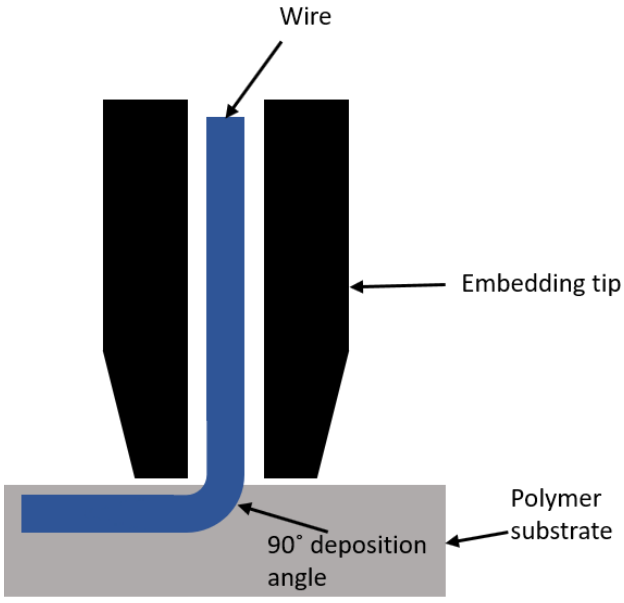

Figure 3: first wire embedding mechanism, configuration used for both ultrasonic and thermal embedding

tip of the ultrasonic horn, as the frequency is usually fixed. This parameter controls the temperature of the wire, for the temperature of embedding must be between the glass transition temperature (Tg) and the melting point of the polymer. The embedder must apply 140 kPa to push the wire inside the polymer. If the temperature of the wire is not above the Tg of the polymer material and the force is not at the specified level, the wire is not going to be embedded, instead the embedder would only drag the wire over the surface. When the wire temperature is too high, three things can happen, (1) the polymer surrounding the wire deforms and when this happens, the build process cannot continue successfully; or (2) the wire stays hot and the polymer does not solidify in time to embed the wire before it pulls out of the surface. The ultrasonic embedding process sees several difficulties, since, to reach the desired temperature, the amplitude must be adjusted to the substrate material. This complicates the process for every time embedding must occur, different parameters must be implemented considering that additively manufactured parts are dissimilar between builds.

The second method explored was Joule heating. This method consists of heating up the wire using its own resistance, while passing current through it (I^2R heating). To heat up the wire, it was connected to a cathode and passed through an insulated tube directed to an anode roller which would be used to push the wire in the polymer. The localized heating that this method has, followed the desired path as it only melts the polymer surrounding the wire. The copper wire (which is used for electrical components) has a resistivity of 1.68 μΩ-cm which makes it difficult for this type of embedding to achieve embedding because currents of 2-10A must be used to perform embedding, depending on the wire diameter. For this reason, this method was not further explored and gave way to the third method.

Thermal wire embedding consists in a tool that heats up with an alternating current (AC) cartridge heaters and lays down the wire through the heated section of the embedder. This wire embedding method possesses flaws in the design. Since the wire cannot be locally heated with this method, the entire tool must be heated. Because of this, the tool leaves a foot stamp around

the embedded wire which, in some cases, can deform the polymer enough to impede continuation of the print.

The first iteration of the thermal wire embedding tool consisted of only a heater block that would elevate the temperature of the wire and lay it down in a perpendicular manner against the previously fabricated substrate. This design induced high stresses on the angle of embedding (Figure 3), thus causing breakage of the wire at that section. To solve this problem, a feed motor was introduced to the tool, creating the second iteration. The feed mechanism introduced in this new iteration improved the embedding but did not remove the breakage problem entirely, at high speeds of embedding (~10mm/sec) or when using thick wire (18 AWG wire) the wire would break.

For the third iteration, the embedding would not happen in a perpendicular manner, but in a tangential (Figure 4). This eliminated the breakage problem and increased the upper embedding speed boundary. Using this configuration, embedding was performed up to 10mm/sec without problems. This configuration also has a feed mechanism that contributes to resolving embedding problems at starts and turns, where wires have a tendency to not embed. At the start of the process, the polymer usually does not solidify sufficiently as the tool moves away from the start point. This drags the wire along and instead of embedding the wire, it creates a channel that impedes embedding. The process itself of heating up the wire can have a detrimental effect on the already embedded portion of the wire because of the high thermal conductivity (~400W/mK) of copper.

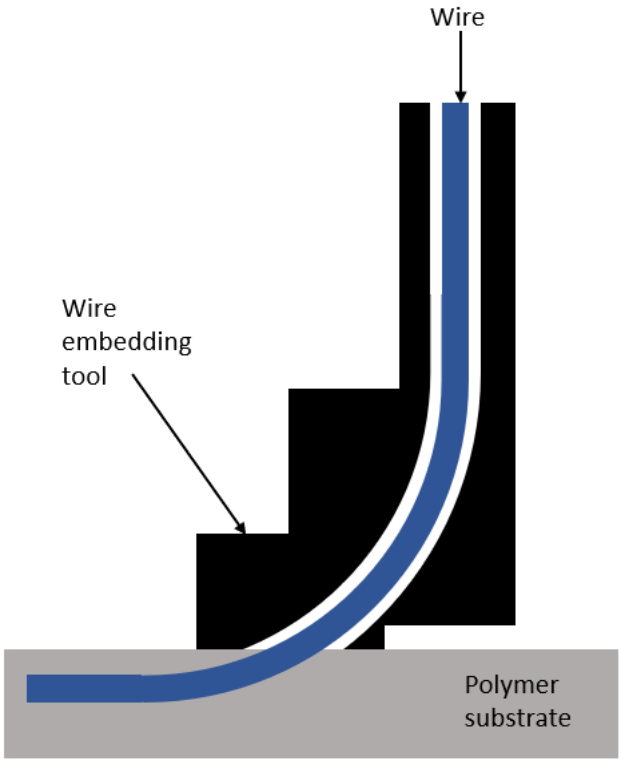

Figure 4: Third wire embedding iteration, features a tangential method of embedding

Heat transfer is higher, and because of the high thermal conductivity, sometimes unembedding of the wire may be observed because the embedded portion of the wire is too hot (Kim *et al*., 2015).

2.5 GLASS-TRANSITION TEMPERATURE

Material extrusion is a technology that uses semi-molten thermoplastics to additively manufacture. For the material to enter the semi-molten stage, it needs to reach its Glass-Transition temperature. At this temperature (it varies depending on the material), the polymer starts to lose its micro glass-like structure and after this point a flowable plastic is obtained. Three things happen for the flowability to take place: there is long range molecular motion, chains are subjected to segmental motion and they experiment rotational freedom. Other properties of the plastic change upon reaching the glass transition temperature. These changes include thermal conductivity and stiffness values.

2.6 SHAPE MEMORY EFFECT ON POLYMERS

All polymers have a property called a shape memory effect. Every type of polymer has its own shape memory effect that, through the input of temperature, stress and strain, will have a different behavior. Voit *et al.* explain the differences that a thermoplastic and a thermoset have about the shape memory effect (Voit *et al*., 2010). They explain that thermoplastics usually do not have a very high recovery rate, in fact the original shape can be entirely deformed, especially in cyclical loadings at high strains whereas some thermosets can have almost full recovery under the same conditions. This is because thermoplastic polymers rely only on physical crosslinks of the polymer chains such as local crystallinity regions and chain entanglements due to the lack of chemical covalent crosslinks that are available in thermosets.

Gall *et al.* describe the driving mechanism of shape memory effect which is entirely dependent on the temperature at which deformation took place. The low entropy state created and subsequently frozen during the thermomechanical cycle (Gall *et al*., 2010) is the primary driving force for shape recovery in polymers. If, when deformation occurs, the hard polymer regions are

deformed below the glass-transition temperature the initial shape recovery becomes easier. This means that deformation above glass transition temperature can induce a permanent deformation on the polymer (Behl and Lendlein, 2007).

It is important in this project to have the knowledge of the shape memory effect in polymers. For actuator applications with SMAs that are activated through temperature, the shape memory effect of polymers plays an important role since recovery of the actuator relies upon stiffness of the polymer. If the polymer is permanently deformed by the heat induced in the wire, then the polymer loses the required properties for actuation.

2.7 SHAPE MEMORY ALLOYS

Shape memory alloys are types of alloys that change shape when a stimulus is applied to them. The stimulus can either be thermal, electrical or magnetic. The two main elements used as a base for SMAs are copper and titanium. Copper-zinc-aluminum and copper-aluminum-nickel are some examples of copper-based SMAs that are more commonly used because of their ductility. These alloys are activated through thermal stimulus. Nickel-Titanium (NiTi) alloys have a thermal or electrical stimulus. This is because the high resistivity of this system acts as a resistance heater, and thus, both electrical and thermal stimuli can activate the shape memory effect. Other alloying elements are added to the NiTi system to increase or decrease the temperature of activation. Cobalt-nickel-aluminum and nickel-magnesium-gallium are some shape memory alloys that are activated through a magnetic stimulus. The shape memory effect is due to a rearrangement of the molecules in the organization of the microstructure of the alloy named as a "Phase change" and shape memory alloys contain two solid phases, a high temperature phase (Austenite) and a low temperature phase (Martensite). This phase transformation happens as a result of the distortion of the lattice by shear.

The austenite phase generally has a cubic crystal structure while the martensite phase can have tetragonal, orthorhombic or monoclinic crystal structure. The martensite crystals can be oriented in different directions, this is called detwinned martensite. When the orientation is

dominant to a specific direction, it is called twinned martensite (Lagoudas, 2008). The Austenite phase assumes the programmed shape and whenever the alloy is heated to reach this phase, it will reshape into the austenite shape. When the alloy is cooled down, the alloy comes back to its Martensite phase. If any deformation should happen in the Martensite phase, the Austenite phase will reshape the alloy to its programmed shape. The shape change is also accompanied by a significant force (Rediniotis *et al*., 2002).

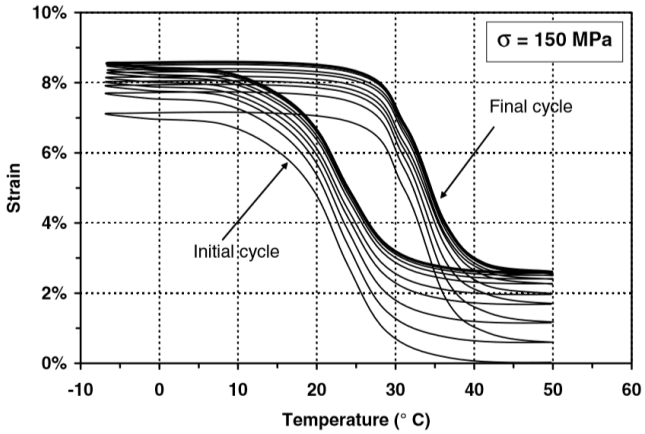

Figure 5: thermal cycling loadings at a constant stress of 150MPa (50 repetitions). Adapted from 'Shape memory alloys: modeling and engineering applications (p 16),' by D. C. Lagoudas, 2007, New York, NY: Springer. Copyright 2008 by Springer Science+Business Media, LLC. Reprinted with permission

According to Lagoudas in his book Shape Memory Alloys Modeling and Engineering Applications, the shape memory activation cycle sees some sort of hysteresis along subsequent activation of the alloy (Figure 5). This means that repeated activation of the wire tends to reduce the motion that the Austenite phase induces on the alloy to a point where it reaches a steady state, meaning that subsequent activations will induce the same shape shifting. (Lagoudas, 2008)

The SMA wire used in this study was Flexinol and was developed by the company Dynalloy (Dynalloy, 2018). The company manufactures SMA wires with two different activation temperatures. Activation takes place over a range of temperatures described in Figure 6. This range of temperatures govern the change of phase of the alloy.

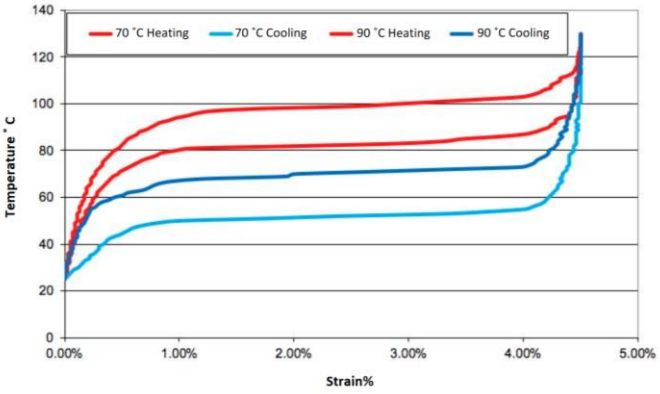

Figure 6: Temperature vs strain graphs for Flexinol SMA wire.

2.8 HEAT TRANSFER THEORY

Heat transfer is the science branch of the thermal sciences that studies the energy transfer through heat transfer. The energy transfer through heat transfer is done by differences of temperature and the direction is always towards the lower temperature, complying with the second law of thermodynamics. The following equation describes the total heat transfer from a hot to a cold medium with no work associated, assuming no heat losses and constant specific heat of the material:

$$Q = mC_v\Delta T \tag{1}$$

Where Q is total heat transfer in joules, m is the mass of the object, Cp is the specific heat of the object and the ΔT is the temperature difference over which heat transfer is occurring.. This equation is converted to rate when an open system is considered. The heat transfer rate (in Watts) then becomes $\dot{Q}$ and mass is transformed into mass flow rate.

There are three types of heat transfer, including conduction, convection and radiation. The conduction heat transfer is when the higher energetic particles transfer this energy to the adjacent lower energetic particles through the interactions between them. Conduction can happen between solids mostly; however, liquids and gases are not exempt from experiencing conduction heat transfer. The properties of materials that play a big role in conduction heat transfer are the thermal conductivity of material, the specific heat and the density of the material. The thermal conductivity is a material property that determines the rate of heat conduction through a medium (i.e. The higher the thermal conductivity the better thermal conductance). The specific heat tells how much energy can a kilogram of material store. The density, in combination with the thermal conductivity and specific heat determines the thermal diffusivity, which is a property that tells how fast heat propagates through the material. The following equation describes the conduction heat transfer, assuming constant thermal conductivity:

$$\frac{\partial^2 T}{\partial x^2} + \frac{\partial^2 T}{\partial y^2} + \frac{\partial^2 T}{\partial z^2} + \frac{\dot{q}_{gen}}{k_{wire}} = \frac{1}{\alpha}\frac{\partial T}{\partial t} \quad (2)$$

This equation is called the general conduction equation and it describes the heat conduction across all dimensions with a time dependence. This equation can be simplified by different assumptions such as one-dimensional heat transfer when the application allows for it, or steady state assumption when it is reached fast enough that the difference would be negligible. This equation is available in cylindrical coordinates and in spherical coordinates also for the analysis of different shapes.

Convection heat transfer is the mode of energy transfer that utilizes fluid in motion to transfer heat. The absence of fluid motion gives pure heat conduction, not convection. Convection is governed by the heat transfer coefficient that relates heat transfer to the fluid properties, the velocity of the fluid and the surface over which the fluid is moving. This heat transfer coefficient is denoted as h and is in $W/m^2 \times °C$. The Convection heat transfer mechanism can be separated into two types: forced convection and natural convection.

Forced convection is when a fluid is forced onto a surface or along it to transfer the heat in or out of the surface. This can happen with the fluid being inside a tube or outside, on the surface of things. This mechanism is commonly used in car radiators, computers and chillers for cooling purposes.

Natural convection is the mechanism that happens as a result of buoyant forces creating a current of air around the hot objects. If an object is hot, the heat will transfer to the adjacent layer of fluid. As a result of the temperature increase of the fluid, its density drops (since density of gases is inversely proportional to temperature at constant pressure). The drop of density moves the fluid up, making way of colder fluid to touch the hot object. This process is repeated until the object reaches the temperature of the surroundings. This type of convection will not only depend on the properties of the surrounding fluid and the hot solid, it will also depend on the temperature of the surface of the solid.

The different types of convection, although depend on the same things (surface of solid, velocity and properties of fluid), are analyzed differently. The following equation describes the heat transfer rate in W for convection:

$$\dot{Q} = hA_s(T_s - T_\infty) \tag{3}$$

Where h is the heat transfer coefficient, A_s is the surface area of the solid, T_s is the temperature of the surface and T_∞ is the temperature of the surrounding fluid. What changes for every type of convection heat transfer is the heat transfer coefficient. The heat transfer coefficient is typically calculated using empirically determined equations for a specific case of convection.

Radiation heat transfer is a mechanism that, unlike conduction and convection, does not use a physical medium for acting. The changes of electronic configurations of the molecules in an object that produce an electromagnetic wave (photon) is the driving mechanism for radiation heat transfer. When this radiation is increased by the heat in an object that is when radiation heat transfer happens. This mechanism of heat transfer is described by the following equation, where ε is the emissivity of the surface and σ is the is the Stefan-Boltzmann constant:

$$\dot{Q} = \varepsilon\sigma A_s({T_s}^4 - {T_\infty}^4) \tag{4}$$

The emissivity is a factor that determines how much does a surface emit in comparison with a blackbody which is considered an "ideal radiator". This emissivity ranges from 0 to 1, 1 being the emissivity of a blackbody. The Stefan-Boltzmann constant involves the blackbody radiation and it defines the power per unit area that a blackbody emits as a function of its thermodynamic temperature (Cengel and Ghajar, 2015).

2.9 MECHANICS OF MATERIALS BENDING STRESS

In mechanics of materials, there are different types of analyses that are available for determining specific stresses on materials. These types of analyses describe the force-driven deformation of materials and give useful information for quality and application-specific design. To perform these analyses, it is important to determine several assumptions for the analysis to work depending on the application it is going to be used for. In this study, only a bending stress analysis was performed to determine the dimensions that a part must have for actuation to happen. To conduct the analysis, the polymer's stiffness, the force that the wire exerts on the polymer and the distance that the determinant force will exert on the polymer, must all be considered.

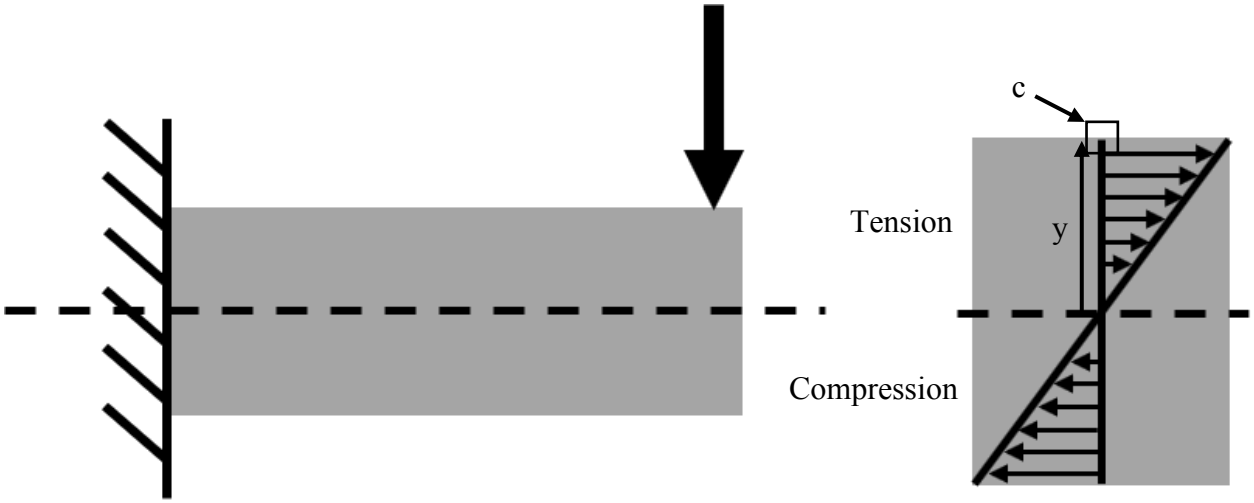

Figure 7: (a) Beam in bending stress with left side totally constrained; (b) Stress distribution upon beam

In Figure 7 (a), there is a visualization of a beam in bending stress with one end totally constrained and the other one free to move. Figure 5 (b) shows a cross-section of the beam, including the stress distribution across the beam.

It is seen in Figure 5 that when a beam experiences bending, it is subjected to compressive and tensile forces perpendicular to the bending force applied, distributed across the thickness of the beam. The maximum bending stress is located at the outmost positions of the beam (i.e. the top and bottom surfaces). As a bending force is applied downwards onto a beam, it will bend on the direction of the force applied. This bending will stretch the top of the beam and compress the

bottom. There is a region where no stress is seen when bending stress is applied, and it is called the neutral axis. All calculations are developed through analysis of the above and below neutral axis stress. If enough force is applied that will make the stress on the beam surpass yield, the beam will fail. The maximum stress that can be applied is determined by the following equation which describes the linear variation of stress from the neutral axis:

$$\sigma_{bending} = \frac{My}{I} \tag{5}$$

Where σ is the maximum stress applied, M is the Moment applied on the beam (force times distance), y is the distance from the neutral axis where the analysis is going to take place and I is the polar moment of inertia which comes from the cross sectional area of the beam.

If the y in Equation (5) is maximized (meaning that y is placed in the outmost distance from the neutral axis called c), it is possible to say that maximum stress is reached at that point. With the use of the polymer's stiffness and the wire's force of activation, it is possible to determine some dimensions for constraining the design to grant motion to the actuator (Budynas *et al*., 2015).

2.10 SHAPE MEMORY ALLOY HYBRID COMPOSITES

Hybrid composites with shape memory alloys and thermoplastic polymer have been investigated in the past with the objective to achieve improved structures that would be useful for different applications. A study was conducted by Meo *et al.* on increasing the impact strength of composites by adding shape memory alloy wires to the composite. They concluded by comparing the strength of conventional composites and the SMA composites and finding out that embedding the SMA wires into the composite results in an overall strengthening of the composite (Meo *et al.*, 2013). Manufacturing of composites was performed through conventional composite manufacturing (hot pressing). Hybrid SMA composites have also been used as adaptive materials for the control of structural acoustics (Rogers, 1998). No research has been conducted in hybridizing additive manufactured parts with SMA wire addition.

CHAPTER 3: ADDITIVELY MANUFACTURED ACTUATORS

3.1 CONCEPT

Actuators are usually designed using solenoid magnetic motion or other types of motion mechanisms (i.e. pneumatic). Systems that use these kinds of actuators must be designed according to the shape and size of the solenoid; this constrains the design and increases its size depending on the driving mechanism of the motion. Another constraint imposed by actuator designs is their power input; if it is pneumatic, it needs compressed air, air hoses and connectors, while if it is electrical, it needs a power supply, controller, and electrical connectors to be functional.

AM usage leads to the manufacturing of custom shapes. These shapes, enhanced by SMAs can potentially reduce the pneumatic/electrical requirements of actuators in systems. They can also potentially reduce the weight of the actuator. The SMA embedded in the thermoplastic polymer is intended to behave as a solenoid or other mechanism of actuation. The SMA's phase change at activation will be used to induce motion on the component, and when deactivation occurs, the polymer's stiffness is intended to move the component back to its original position/shape. This way, actuation can be repeatable and can be used for long lasting applications.

For actuation, the SMA is intended to be connected to a current source for activation. For this, the correct current quantity must be applied. If the current input is not correct, several problems can arise involving the temperature of the part. As a result of a current input that would elevate the wire beyond the T_g of the surrounding polymer, overheating may occur which will affect the actuator's ability to go back to its original shape, removing repeatable motion. A study regarding the current-temperature relation was performed in this work to determine the current necessary to activate the wire, depending on the length of the embedded wire and the surrounding mass of polymer used for the actuator.

The shape memory alloy (SMA) described above has the capability not only to move the polymer, but also to sense the temperature of its surroundings. In addition to predetermined

actuation, additively manufactured actuators using SMA wire for motion can be also utilized as sensor-actuator components. These complex components are able to react to a certain temperature input by moving. This motion can be used for closing circuits or other range of applications.

In this work, a modified Lulzbot TAZ 5 desktop material extrusion system was used to fabricate the actuators. The machine has an included wire embedding tool that is controlled through marlin v1.1.5 which is the motion control software of the Lulzbot TAZ 5. This wire embedder uses thermal embedding with tangential method and a feeder mechanism. The tool attached on the machine can be observed in Figure 8 where the tangential embedding and feeder mechanism is described.

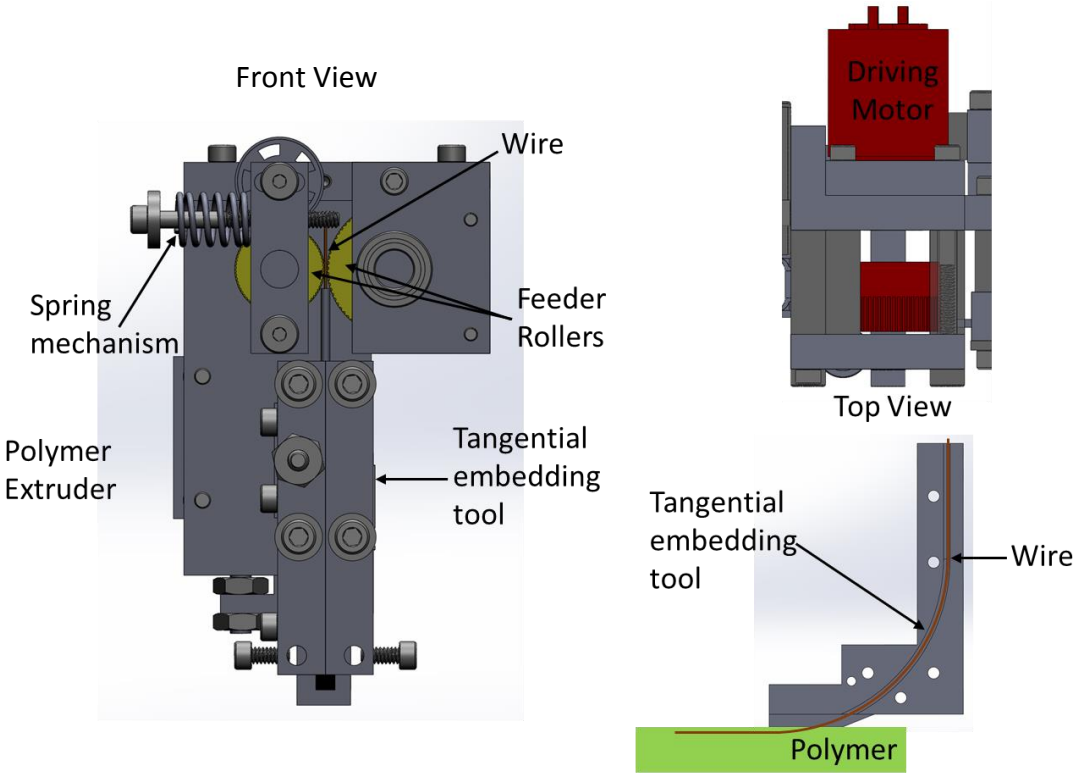

Figure 8: Wire embedding mechanism. The front view shows the feeding mechanism that forces the wire through the hypodermic tube to be directed to the tangential embedding path.

Several factors had to be addressed to finalize the method for designing actuators such as: (1) temperature of actuation, (2) polymer stiffness, (3) temperature of fabrication, (4) bonding force between wire and polymer, and (5) repeatability of actuation. All these factors were analyzed and used for the development of the fabrication methods for additively manufactured actuators.

3.2 MATERIAL SELECTION

The materials used for the creation of actuators are: a thermoplastic elastomer and a SMA wire. For the activation, a nickel-titanium (NiTi) wire was used. The actuation relies upon the motion of the activated wire to initiate movement. To recover to the original position, the polymer's stiffness will act on the inactivated wire. The process described before is expected to be repeatable through the life of the actuator.

The shape memory alloy selected must have an activation temperature below the glass transition temperature of the polymer used for manufacturing. If the embedded wire sees a higher temperature than the glass transition temperature of the polymer, the stiffness of the polymer may become compromised due to the permanent deformation that happens if the polymer is deformed at above its glass transition temperature. This effect would prevent any further actuation as it would never recover to the inactivated position of the actuator. To activate the actuator, the wire should be energized through temperature or current (which would increase the temperature of the wire). In this study, current is the activation input that will be utilized because it is possible to quantify the heat and temperature that are to be reached for activations.

As current will be the main input studied, it should be noted that the wire will act as a resistance heater. This means that the heating is dependent on the material surrounding the wire and resistivity of the wire (i.e. if the wire is long it will need more current to reach activation temperature than for a short wire). To obtain a correct current input, it was necessary to model the heat transfer to include the thermal and electrical properties of the wire, as well as the material surrounding the wire and the temperature to be reached (activation temperature). With this model, overheating will be prevented by the control of current input with the calculated current values. This will prevent any damage that overheating may induce on the polymer's stiffness.

The polymer selection criteria is driven by the modulus and glass transition temperature of the polymer in combination with the SMA properties. The desired properties are a polymer with a T_g that would be higher than the activation temperature of the wire, as well as a low modulus of

the polymer that would allow for broad design of actuators in combination with the SMA wire selected.

To allow for the actuator to move, design must consider the polymer stiffness and the force of motion of the wire. The correlation between both of these properties in an equation can result in dimensional boundaries that would allow for motion of the actuator. The equation that can correlate these properties is a bending stress equation.

Both properties described to be critical to the actuation are not very common to be present in polymers at the same time. Some polymers exhibit a low stiffness (~15MPa) but it comes accompanied by very low T_g (-65°C) meaning that the activation of the wire will permanently deform the polymer. Other polymers have a T_g that surpasses the activation temperature of the wire, but the wire's motion force cannot overcome their stiffness and thus cannot be used.

3.3 WIRE EMBEDDING

The embedding methodology used for this study was not automatic. Wire was embedded on the surface of the polymers through manual interaction. This manual interaction consisted of manually placing the wire on top of the substrate and manually heating the wire using a resistance heater. Simultaneously, load is exerted down upon the wire until the temperature of the wire

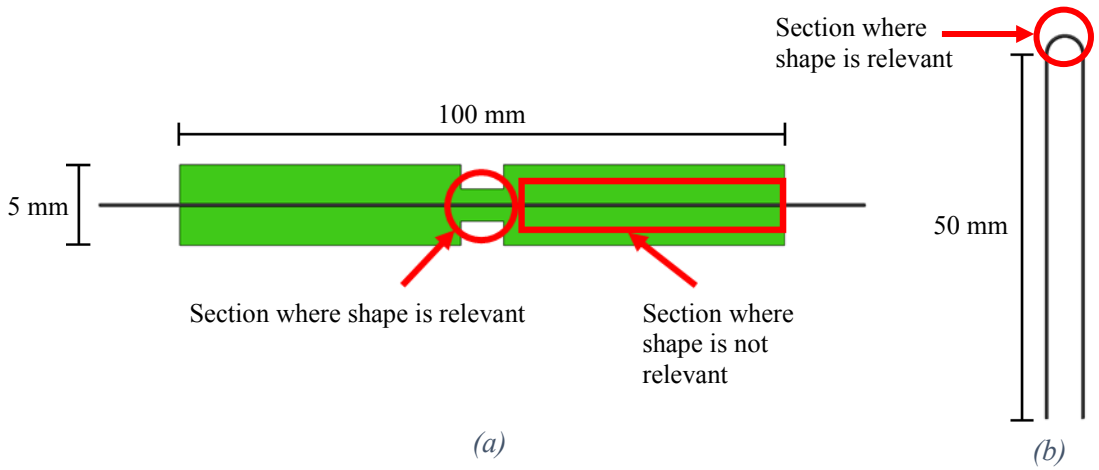

Figure 9: (a) Part designed with two highlighted sections, one with relevant shape and other with not relevant shape. The relevant shape was not embedded, as embedding would remove the shape induced; (b) Wire prior to embedding with induced shape, relevant for actuation.

surpasses the T_g of the polymer and the force applied inserts the wire onto the molten polymer. When the polymer solidifies, the wire is captured by the polymer entirely.

Figure 9 shows a design made for actuation. This part was designed to have a bend on the middle. The wire had an induced shape for the activated phase (Austenite) shown in Figure 9 (b). This section of the wire where the shape memory effect is relevant because the austenite shape of this section is what drives the motion of the actuator. The wire in the polymer, shown in Figure 9 (a), is only embedded on the sections highlighted, where the shape memory effect is not relevant, as it is not relied upon for actuation, to prevent loss of the induced shape. When the print is continued, the following layer covers up the section of the wire that was not embedded.

Although there are several methods for automatic wire embedding available such as ultrasonic and thermal embedding, both methods elevate the temperature of the wire for embedding to take place. Heating up and deforming the wire reconfigures the austenite shape of the wire, and thus, desired actuation is lost. Figure 10 shows the deformation that thermal embedding induces on the wire. Because of the negative impact of passing the wire through embedders, shown in Figure 10, it was decided to perform embedding manually.

(a) *(b)*

Figure 10: *(a) wire after activation prior to embedding; (b) embedded and removed wire after activation*

3.4 MODELING

For the actuator to move without the activation of the SMA wire causing permanent deformation of the polymer, it is necessary for the wire to reach the activation temperature. Also the force exerted by the wire must be enough to overcome the polymer's stiffness. Using mathematical modeling, it is possible to calculate the temperatures and dimensions required to

have motion of the actuator. These two models were used to determine a final design shown in later chapters.

3.4.1 HEAT TRANSFER

Heat transfer modeling has been performed before to obtain the temperature of electrical conductors (Ilgevicius, 2004). However, assumptions used for that study could not be incorporated in this work because of the difference of thermal conductivity between the materials used. The

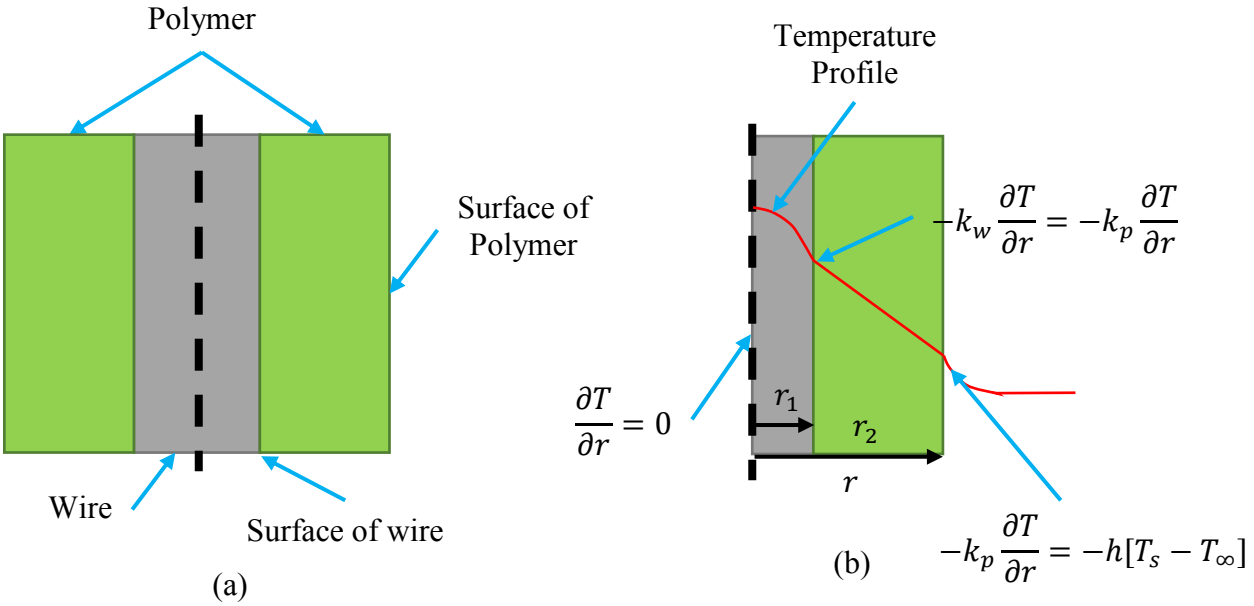

Figure 11: (a) wire in polymer schematic; (b) symmetry assumption with boundary conditions showing the temperature profile

thermal conductivity of copper is 385W/m·K and that of NiTi, which is the alloy used in this study is 18W/ m·K. To obtain the correct current input based on the activation temperature of the wire, a conductive-convective heat transfer model was developed. Two models were created, one simulating a wire embedded within the polymer and a bare wire heated in air. The model for wire in air was created for simplicity of validation.

A cylindrical, insulated resistance heater model was used to simulate the wire embedded in the polymer, the wire acting as the resistance heater and the polymer acting as an insulator. For simplicity of analysis, the model was taken to have symmetry boundary conditions (Figure 11). In

the symmetry boundary, the differential of temperature with respect to distance can be taken to be equal to zero due to the slope of temperature which is equal to zero at the point where $r = 0$.

There is a change of materials on the interface of materials at $r = r_1$, where the slope of the temperature gradient changes due to the change in thermal conductivity ($k_w \neq k_p$); however, the point $x = r_1$ is an equivalent value that can be represented in the following equation:

$$-k_{wire}\frac{dT_{Wire}(r_1)}{dr} = -k_{pol}\frac{dT_{pol}(r_1)}{dr} \tag{6}$$

At $r = r_2$, there is a convective boundary. This means that the part sees convection heat transfer at that point. The type of convection found at this point is natural convection. This point ($r = r_2$) can be shown in the following equation

$$-k_{pol}\frac{dT_{pol}(r_1)}{dr} = h_{nat,conv,pol}[T(r_1) - T_\infty] \tag{7}$$

For the wire in air model, a cylindrical shape with resistance heating was used. The boundary conditions utilized were very similar to that of the wire in the polymer; however, in this case there is no polymer surrounding the cylindrical resistance heater, thus the convective boundary condition was placed on the surface of the wire.

$$-k_{wire}\frac{dT_{wire}(r)}{dr} = h_{nat,conv,wire}[T(r) - T_\infty] \tag{8}$$

Both models were assumed to be in a steady state form for simplicity and one dimensional cylindrical coordinates because usually long wires are going to be used, neglecting heat transfer across the length of the wire and the heat transfer model was taken to be planar (φ is neglected).

$$\frac{1}{r}\frac{\partial}{\partial r}\left(r \cdot \frac{\partial T}{\partial r}\right) + \frac{1}{r^2}\frac{\partial^2 T}{\partial \varphi^2} + \frac{\partial^2 T}{\partial z^2} + \frac{\dot{q}_{gen}}{k_{wire}} = \frac{1}{\alpha}\frac{\partial T}{\partial t} \tag{9}$$

The equation above is the general heat conduction equation for transient, 3-dimensional heat transfer with heat generation on cylindrical coordinates. Since this will be taken to be one dimensional and steady state, the time term and two dimensions can be equaled to zero, resulting in the following equation:

$$\frac{1}{r}\frac{d}{dr}\left(r\cdot\frac{dT}{dr}\right)+\frac{\dot{q}_{gen}}{k}=0\rightarrow d\left(r\cdot\frac{dT}{dr}\right)=-\frac{\dot{q}_{gen}}{k_{wire}}\cdot r\cdot dr \tag{10}$$

If the resulting equation is integrated once and rearranged, it would result to the following equation:

$$\frac{dT}{dr}=-\frac{\dot{q}_{gen}}{k_{wire}}\cdot\frac{r}{2}+\frac{C_1}{r} \tag{11}$$

The constant can be taken to be 0 because of the symmetry boundary condition that whenever $r=0$ then $\frac{dT}{dr}=0$.

At this point of the equation derivations, the analysis has been concentrated on the wire portion of the part. If the polymer portion of the part is considered, the general conduction equation can be used without heat generation and in steady state form:

$$\frac{d}{dr}\left(r\cdot\frac{dT}{dr}\right)=0 \tag{12}$$

If this is integrated twice, the following equation results

$$T(r)=C_1\ln(r)+C_2 \tag{13}$$

When the boundary conditions are applied ($T=T_1\ @\ r=r_1$)($T=T_2\ @\ r=r_2$), C_1 can be obtained with the following equations

$$T_1=C_1\ln(r_1)+C_2 \quad T_2=C_1\ln(r_2)+C_2 \tag{14,15}$$

After both equations are combined and rearranged the following constants result:

$$C_1 = \frac{(T_2 - T_1)}{\ln\left(\frac{r_2}{r_1}\right)} \qquad C_2 = T_1 - \frac{(T_2 - T_1)}{\ln\left(\frac{r_2}{r_1}\right)} \ln(r_1) \tag{16,17}$$

The equation obtained for the polymer section of the part results in the following:

$$T(r) = \frac{\ln\left(\frac{r}{r_1}\right)}{\ln\left(\frac{r_2}{r_1}\right)}(T_2 - T_1) + T_1 \tag{18}$$

Using Equation 6 (previously described) it is possible to relate both equations obtained, the one from the wire with heat generation and the one from the polymer that is surrounding the wire

$$-k_{wire}\frac{dT_{Wire}(r_1)}{dr} = -k_{pol}\frac{dT_{pol}(r_1)}{dr} \rightarrow k_{wire}\frac{\dot{q}_{gen}r_1}{2k_{wire}} = -k_{pol}\frac{T_2 - T_1}{\ln\left(\frac{r_2}{r_1}\right)}\frac{1}{r_1} \qquad (6\rightarrow 19)$$

As both differentials are available through Equations 6 and 18, it is possible to complete the equation above. The first differential corresponds to Equation 6 which is the wire equation and the second differential corresponds to Equation 18 which is the portion where the polymer was considered instead of the wire. Inserting the actual differentials would result in Equation 19. After rearranging and isolating for T_1, which is the temperature at the interface of the wire and the polymer, the following equation emerges:

$$T_1 = \frac{\dot{q}_{gen}{r_1}^2}{2k_{pol}}\ln\left(\frac{r_2}{r_1}\right) + T_2 \tag{20}$$

Where T_1 is the temperature at the interface and T_2 is the temperature at the surface of the part. T_1 is desired since the temperature at the interface between the wire and the polymer is the temperature that drives the motion of the actuator and it must be calculated to input the right amount of current so that the wire can reach that specific temperature.

As T_2 is an unknown value, another equation must be used to express T_2. Equation 8 is a correlation between the convective and conductive boundary conditions at r_2, which is a point where the values of these two sides converge as equals. When in this equation the differential is replaced by the derivative of Equation 18, the resulting equation becomes:

$$-k_{pol}\frac{T_2 - T_1}{\ln\left(\frac{r_2}{r_1}\right)}\frac{1}{r_2} = h_{nat,conv,pol}[T_2 - T_\infty] \tag{21}$$

To obtain T_2 and insert it to Equation 20, it must be isolated:

$$T_2 = \frac{T_\infty h_{nat,conv,pol}\ln\left(\frac{r_2}{r_1}\right)r_2 + k_{pol}\,T_1}{k_{pol} + h_{nat,conv,pol}\ln\left(\frac{r_2}{r_1}\right)r_2} \tag{22}$$

With Equation 22 ready and inserted into Equation 20, the equation ends up as follows:

$$T_1 = \frac{\dot{q}_{gen}{r_1}^2}{2k_{pol}}\ln\left(\frac{r_2}{r_1}\right) + \frac{T_\infty h_{nat,conv,pol}\ln\left(\frac{r_2}{r_1}\right)r_2 + k_{pol}\,T_1}{k_{pol} + h_{nat,conv,pol}\cdot\ln\left(\frac{r_2}{r_1}\right)r_2} \tag{23}$$

T_1 is found in both sides of the equation so after rearranging, the final equation results in the following equation:

$$T_1 = \frac{\dot{q}_{gen}r_1^2}{2r_2 h_{nat,conv,pol}} + \frac{\dot{q}_{gen}r_1^2}{2k_{\text{pol}}}\ln\left(\frac{r_2}{r_1}\right) + T_\infty \tag{24}$$

This equation gives the surface wire temperature inside polymer at a steady state with heat generation and one-dimensional heat transfer (r direction).

The term $\dot{q}_{gen}$ refers to a quantity usually in a *per volume* manner. The units of this value are W/m^3, and for the sake of these calculations it can be expressed as follows, since this equation is specifically for heat generation through resistance:

$$\dot{q}_{resistance\ gen} = \frac{\dot{E}_{resistance\ gen}}{V_{wire}} = \frac{I^2 R_{wire}}{\pi {r_1}^2 L} \tag{25}$$

Where I is the current, R_{wire} is the resistance of the wire, r_1 is the radius of the wire and L is the length of the wire. Using Equation 24 and Equation 25, it is possible to obtain a current value for the temperature that is desired (T_1). If both equations are combined the final equation results as follows (Yener *et al*., 2008):

$$T_1 = \frac{I^2 R_{wire}}{2\pi r_2 h_{nat,conv,pol} L} + \frac{I^2 R_{wire}}{2\pi k_{\text{pol}} L} \ln\left(\frac{r_2}{r_1}\right) + T_\infty \tag{26}$$

This same process was done for the equation that applies for wire in air, Equation 8 and Equation 11, when combined give the following equation:

$$-k_{wire} \frac{\dot{q}_{gen}}{k_{wire}} \frac{r_1}{2} = h_{nat,conv,wire}[T(r_1) - T_\infty] \tag{27}$$

When the equation is rearranged and united with Equation 25, it is possible to obtain an equation that would give out a relationship between temperature and current, all other terms are known for this model.

$$T_1 = \frac{I^2 R_{wire}}{2 h_{nat,conv,wire} \pi r_1 L} + T_\infty \tag{28}$$

The natural convection coefficient is a number that considers several variables to be calculated such as thermal conductivity of the fluid, the shape of the hot object and the fluid motion forces that are involved in the heat transfer. In the book Heat and Mass Transfer: A Practical Approach by Yunus A. Çengel (Çengel, 2015), a table is shown with several common shapes for mathematical calculation of the natural convection heat transfer coefficient. The equation for horizontal cylinder is shown below:

$$Nu_{horizontal\ cylinder} = \left\{0.6 + \frac{0.387 {Ra_D}^{1/6}}{[1 + (0.559/Pr)^{9/16}]^{8/27}}\right\}^2 \tag{29}$$

Where Nu is the Nusselt number, Ra is the Rayleigh number and Pr is the Prandtl number. The Nusselt number is a dimensionless representation of the heat transfer coefficient and is represented by the following equation:

$$Nu = \frac{h_{convection} L_{characteristic}}{k_{fluid}} \tag{30}$$

Where h is the heat transfer coefficient, the k is the thermal conductivity of the fluid and the L is the characteristic length of the shape.

The Prandtl number is a property of the fluid surrounding the hot element and the Rayleigh number is the multiplication between the Prandtl number and another dimensionless number called Grashof number. This is a number that describes the ratio between the viscous force of a fluid and its buoyancy force. These two numbers are dependent on temperature of the fluid and are calculated considering it.

The equations described before (equations 29 and 30) can be used to obtain the heat transfer coefficient by replacing the Nu value with the shape-dependent equation presented by Çengel in his book (Çengel, 2015).

3.4.2 Bending Stress

The change of shape of the SMA wire is what enables motion of the polymer/wire system. The polymer must be elastically deformed to obtain motion and for this deformation to happen, the cross-sectional shape must not exceed a certain value according to the bending stress equation (Equation 31). The force in the moment applied, and the modulus of the material are constants determined by the SMA wire and the polymer, respectively. In the equation, only dimensional terms are left that can help in determining the shape of the actuator for deformation to be possible.

According to mechanics of materials theory, the stress needed for deformation to occur must be higher than the modulus of elasticity of the material being deformed. For this analysis, a

u-shaped part was analyzed to move from u shape to straight. Figure 12 shows a schematic of how the part is intended to move and the boundary conditions used for this analysis.

$$\sigma_{deform} = E_{pol}\varepsilon = \frac{Mc}{I_x} \tag{31}$$

The equation above is a bending stress equation where E is the modulus of elasticity, M is the moment created by the wire in force times distance, C is the distance from neutral axis and the I_z stands for the polar moment of inertia. Through this equation, it is possible to obtain dimensional characteristics of what the cross-sectional area of the actuator should be.

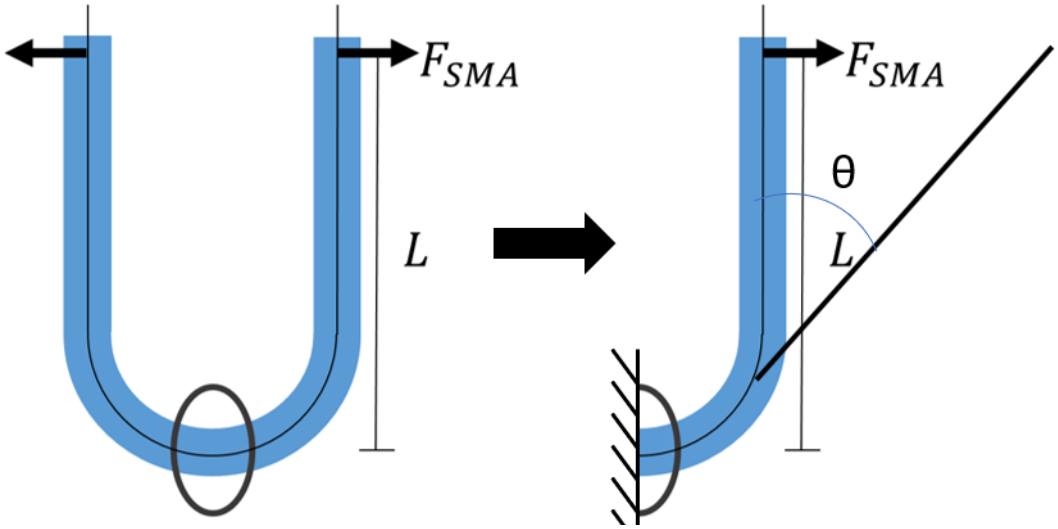

Figure 12: Bending stress analysis with assumption of fixing the middle section of U shape

Since the polar moment of inertia is dependent on the shape of the part to be analyzed, two cases will be studied, one with a rectangular cross-sectional area and one with a circular cross-sectional area. The rectangular shape was selected because of the simplicity of the polar moment of inertia calculation to obtain the dimensional constraints. The circular shape was selected to validate the calculations for the heat transfer model.

The rectangular cross-sectional area has an I_x across the neutral axis represented by the equation below

$$I_x = \frac{bh^3}{12} \tag{32}$$

With Equations 31 and 32 combined, a dimensional relation can be found to constrain the design of actuators to a specific set of dimensions:

$$\boxed{E_{pol}\varepsilon = \frac{12Fd}{bh^2}} \tag{33}$$

Where F is the sideways motion force applied by the wire, d is the maximum distance between the force and the fixed point (Figure 12), b and h are dimensional characteristics of the part and E is the modulus of the polymer.

The circular cross-sectional area has a different I_x which is represented by the following equation:

$$I_x = \frac{\pi D^4}{64} \tag{34}$$

And when combined with Equation 33 and some rearranging, it results in the following:

$$\boxed{E_{pol}\varepsilon = \frac{32Fd}{\pi D^2}} \tag{35}$$

With these two equations, it is possible to obtain an approximate dimensional value, as F is the force value that the manufacturer specifies, to constraint the design of actuators. Figure 13 shows the cross-sectional shape of the part with embedded wire on both configurations, cylindrical and rectangular cross-sections.

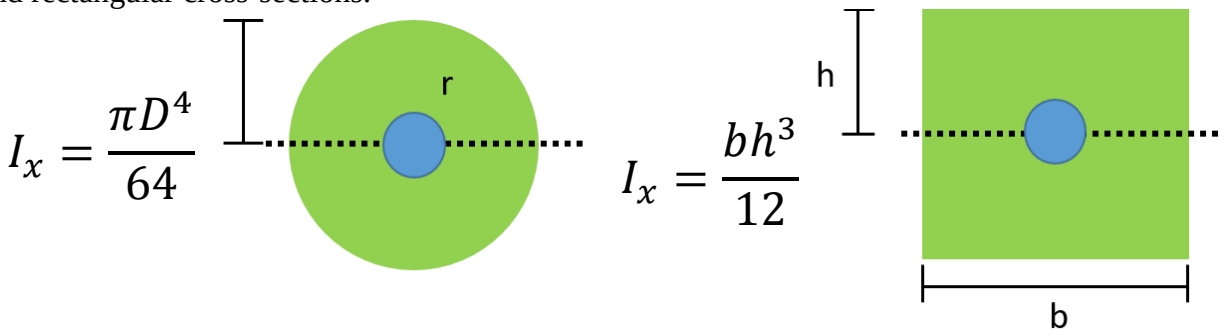

Figure 13: Cross-sectional shape with polar moment of inertia for both analyzed shapes

3.5 LIFE OF ACTUATOR

The life of the actuator will be limited by how the wire behaves within the polymer, how the bond gets affected and how the polymer gets affected by periodic activation. Another factor that will affect the life of the actuator is how fast the cycles be reproduced. This will be determined by how fast the polymer dissipates heat. This factor is essential because permanent deformation may happen if not enough heat is dissipated before any subsequent activation happens. The actuator's size does not allow for thermal management to be designed upon it. Results from several experiments show that thermal buildup is not a problem in the actuator designed.

To determine these factors, a series of tests were performed. A test where the current calculated was cyclically applied to the wire embedded in the part with calculated cross-sectional area was performed. Another test was implemented where temperature was recorded to obtain the time it takes for temperature to decrease to room temperature. By recording the motion through cyclical current input to the wire, the motion is expected to decay the more cycles it goes through as heat accumulates in the polymer.

CHAPTER 4: EXPERIMENTAL METHODOLOGY

4.1 ADHESION TESTS

Three polymer materials were investigated for this project. A seen in Table 1, the materials that qualify best for this application are bottom three that will be described here. The Ninjaflex material is a thermoplastic polyurethane (TPU) manufactured by Fenner Drives. This material showed low stiffness (~12MPa) that could be useful for manufacturing actuators. The ABS/SEBS material is a polymer blend between Styrene-ethylene-butylene-styrene (SEBS) and Acrylonitrile-Butadiene-Styrene (ABS) that was produced by Dr. David Roberson in the W.M. Keck Center for 3D Innovation at the University of Texas at El Paso (Siqueiros *et al.*, 2016). This polymer blend showed low stiffness (~15MPa). The other material is called Plasticized Copolyamide Thermoplastic Elastomer (PCTPE). This material has exhibited low Modulus (75MPa) that would allow still for motion induced by the wire. The low modulus was determined by the calculations performed that would show an allowable motion of the part with the force of the activation of the wire.

The adhesion of the wire to the polymer was measured because for actuation to happen, it is necessary for the wire and the polymer to act as one single piece; to be adhered completely in such a way that if the wire moves, the polymer will move and if the polymer moves, the wire will move with it. For this reason, it was necessary to determine the strength of the bond between SMA wire and polymer.

Figure 14: Specimen for adhesion test with embedded wire at the middle of fabrication

The adhesion was tested by creating a specimen with an embedded wire for tensile testing. The specimens had 50mm of wire embedded at half print (1.5mm) of the print so that the specimen would have a wire surrounded entirely by polymer. Figure 14 shows the kind of specimen that was utilized with the specifications listed above. This specimen was developed for the sole purpose of testing the adhesion of the wire to the polymer, as there is no standard for this. After the five specimens were created for testing, a single fiber pullout test was conducted on every specimen resembling what DiFrancia *et al*. did for determining addition of a fiber in a matrix (DiFrancia *et al*., 1996). Each specimen was clamped as shown in Figure 15, the wire to the top clamp and the polymer part to the bottom clamp, ensuring that the embedded wire was not being grabbed by the clamp. This test was conducted at 2mm/min of pulling speed replicating the test that DiFrancia *et al.* performed. This test gives out a chart of extension vs force and the curve will determine the forces required to overcome the bond between the wire and polymer. The tensile testing was conducted in an Instron 5880 machine with a 500 kN load cell that has a ±0.25% accuracy. The graphs reported were in a load vs extension manner as no method of measuring strain was available.

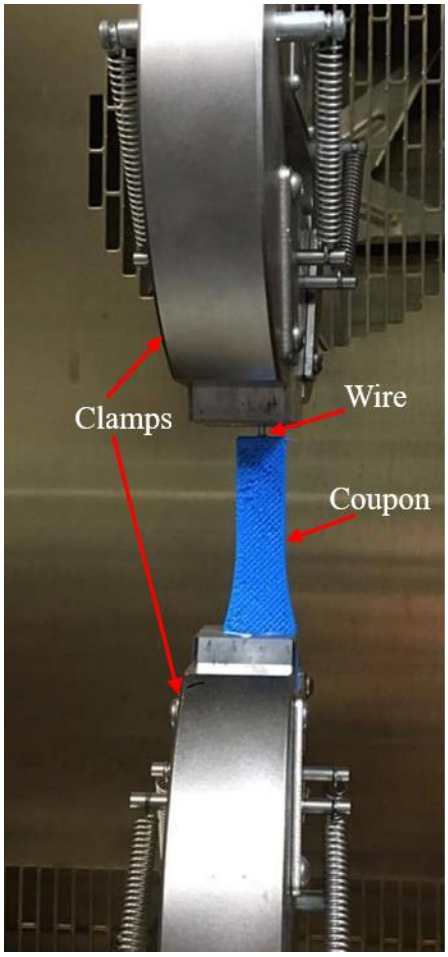

Figure 15: Single-fiber pullout test on TPU specimen

4.2 MODELING VALIDATION

Experiments were performed to validate the models described previously. Two models were used for this study, a heat transfer model and a bending stress model. With these two models, it was intended to achieve actuation via correct current input in the wire and to achieve recovery

of initial shape through the stiffness of the polymer. The validation methods will be discussed in the following sections.

4.2.1 HEAT TRANSFER

The heat transfer model was validated with infrared monitoring of the cylindrical parts that were modeled and with current data acquisition from the power supply. Through the calculations, a current value was collected. This value was then analyzed and compared with the temperatures provided by the manufacturer in a strain vs temperature graph.

The wire in air model resulted with the wire reaching 60°C (with 0.53A applied current), which is the temperature at which activation starts. For the wire in polymer model, only 0.46A of applied current was required to reach 60°C. The lower current is because the polymer is acting as an insulator; thus, heat dissipation is smaller.

For the validation of the wire in air model, a wire of 100mm in length was used, and for the model of a wire in polymer, a wire was embedded on the center of a 3mm diameter cylinder of 100mm in length made from the PCTPE polymer. Both were clamped on both ends inside a controlled chamber to prevent air flow that could compromise the validation. To record motion

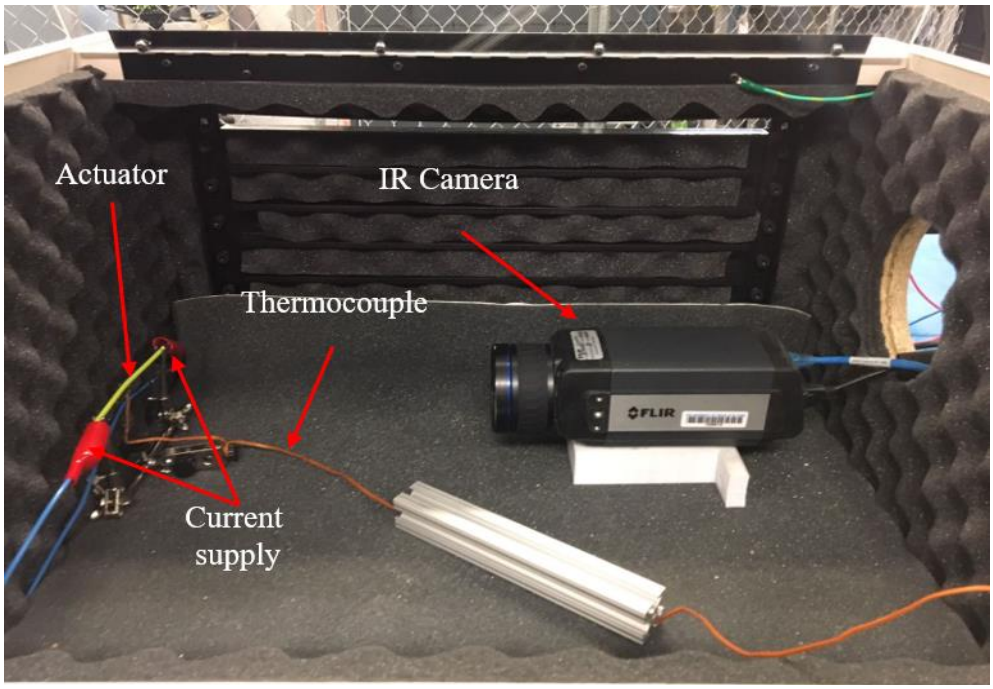

Figure 16: Validation tests setup with IR camera, thermocouple and clamped part

and temperature, a FLIR 580 IR camera was placed 300mm from the part and the emissivity used was 0.2 which was taken from literature (Da Silva *et al*., 2016). For current input, both ends of the wire were connected to a 9115 BK precision programmable variable power supply that can record the current and voltage applied. Figure 16 visually demonstrates the testing setup created for this validation. The thermocouple attached to the part was to monitor the temperature of the polymer while the test was taking place.

The tests conducted consisted of ramping up the voltage up to a peak with free current flow. This way, voltage is on a constant increase while the current increases depending on the resistivity of the material and the voltage applied. As the SMA material changes resistivity when reaching activation temperature, the curve obtained from this test can be used to determine when the wire is activated without having to look at temperature. This test was conducted for four different peak voltages for each of the models: 0.6V, 0.8V 1.0V and 1.2V for the wire in air model and 0.8V, 1.0V, 1.2V and 1.4V for the wire in polymer. The ramp consisted of reaching the specified voltage within 2 min. The current vs time plots obtained were used to compare with the calculated currents and analyzed for validation purposes.

Another test that was implemented was the same ramp but using the same wire for 5 times to determine if the input of current would affect the behavior of the phases of the wire in following cycles. This test was reproduced for the same voltages that were specified before. This test was only conducted for the wire in air model since this was to identify if the wire goes through any change when heated subsequently.

4.2.2 BENDING STRESS

The bending stress model was validated by creating a part with the dimensions that were specified by the calculations in the model. In this case, for a cylindrical part, 2 mm of diameter was calculated to enable motion of a 101.6 mm wire that would bend in the middle (at 50.8mm). Figure 17 shows the reconfiguration motion that the wire should have when activated. For a rectangular cross-sectional area, the values that were calculated resulted in $bh^2 \leq 19.2\ mm^3$. This means that the base of the cross-sectional area times the square of the height must be equal or more than 19.2 mm^3. The parts created with these numbers were then subjected to current, and motion would indicate that the model was correct.

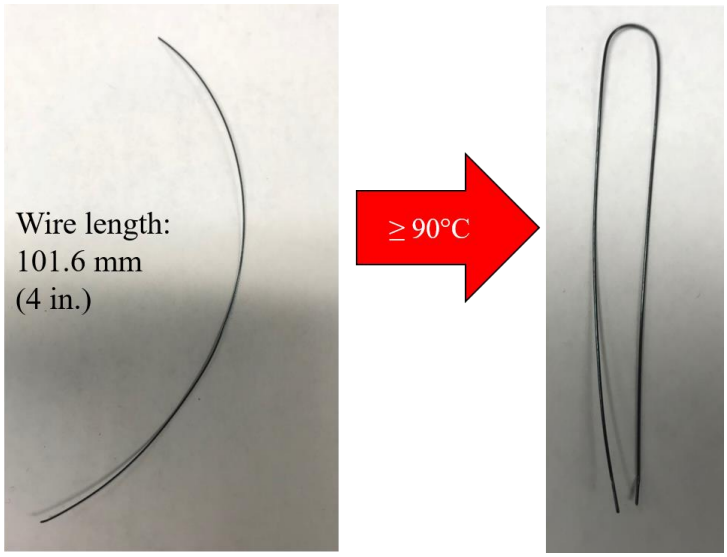

Figure 17: wire programmed to a curved shape from straight for, when activation happens, it will try to assume the shape programmed.

Table 2: shows the results of the calculations for bending stress analysis.

Cross-sectional shape	Dimension	Measure
Circular	D	1.5 mm
Rectangular	bh^2	19.2 mm^3

4.3 REPEATABILITY TESTING

These tests were conducted with the calculated current for reaching the activation temperature on the parts with dimensions calculated. The tests consisted in periodically passing current through the wire, over a period of time. This periodical current pass through would activate and deactivate the wire. Two parts were fabricated, one cylindrical and one rectangular, with the dimensions previously show in Table 2. The current used to test these parts was obtained from the voltage ramp to validate the heat transfer model of wire in polymer (1.5A). This current is where the wire was already fully activated. The test consisted of two different cycle times: one second current on and 10 seconds current off and, one second current on and 15 seconds current off to determine what is the smallest amount of time between cycles without compromising displacement. The test was monitored with a K-type thermocouple embedded close to the wire to record temperature on a NI-9214 temperature data acquisition module with a cDAQ-9171 chassis and with a Microtrak 7000 laser displacement sensor for recording the motion of the wire. The KEPCO ABC 25-4DM programmable power supply was controlled with an Arduino MEGA board that was programmed to cyclically open and close a relay to input and cut current at the rates determined before. The setup used to test the cyclical life of the actuator is shown in Figure 18.

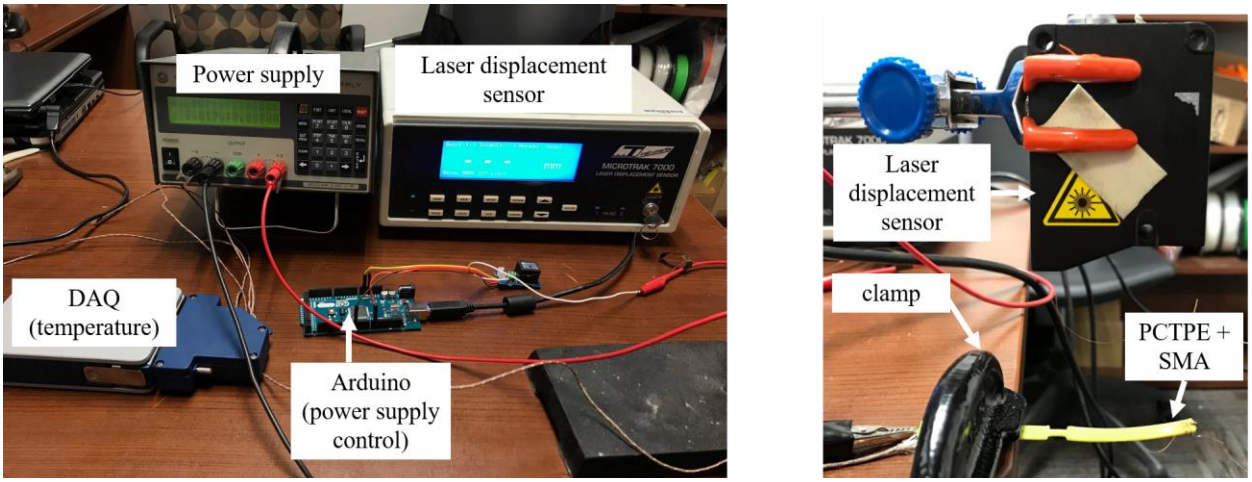

Figure 18: Setup for testing the repeatability motion. It includes displacement sensor, temperature data acquisition device and power input device.

CHAPTER 5: RESULTS AND DISCUSSION

5.1 ADHESION TESTS

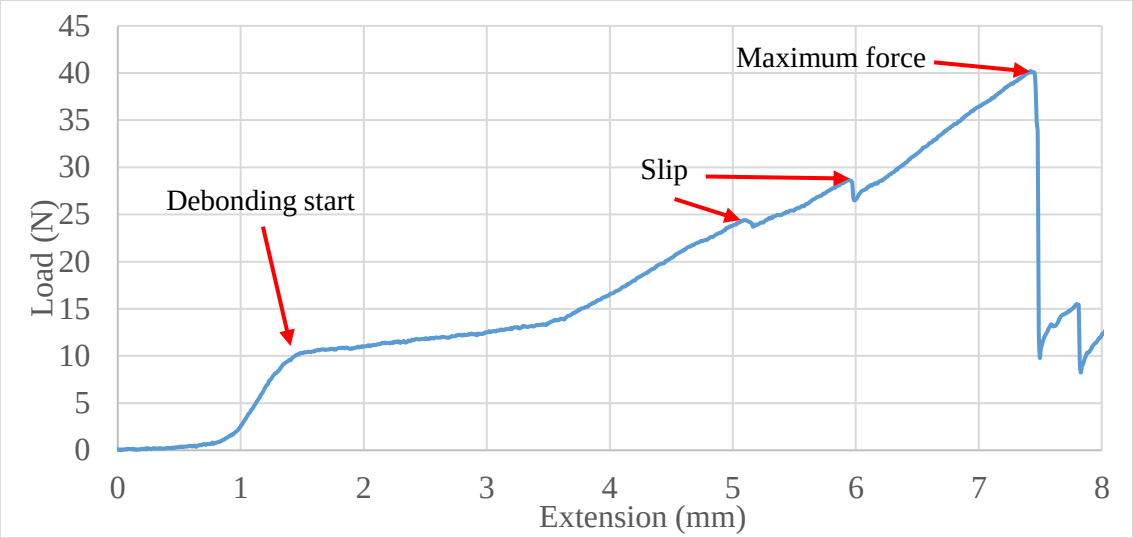

Figure 19: Load vs extension curve of the wire embedded in TPU. Curve shows a debonding start point and several sections where wire slips from the polymer.

The tests were performed for three different materials: TPU, ABS/SEBS blend and PCTPE. The TPU material was the first polymer to be used in this project. Testing of the bonding strength was conducted after determining that the SMA wire would debond from the polymer as the part was being removed from the build platform. Figure 19 shows the debonding curve (force vs extension) for TPU and the Flexinol wire. This curve shows that at 10N, debonding starts, and that through the test, some slip is seen from the wire inside the polymer. The force reported in these values showed that this combination of polymer-wire was not viable for this project (TPU-Flexinol). However, other alternatives were explored such as mechanical and chemical surface treatments of the wire to increase the bonding between the TPU and the wire. Only one specimen was tested because this was only to determine experimentally what was seen while removing the part from the build platform. The regions where a sudden change happens were considered as slip as Qiu *et al*. mention (Qiu *et al*., 2016).

According to Ghosh and Schiraldi, bonding strength between copper and TPU was increased through chemical surface treatment of the metal that was embedded in TPU. They recorded a bonding strength increase of more than 30 times, from 50N/m to more than 1.5kN, after the chemical treatment. For this reason, this same treatment was reproduced for this application. 3-aminopropyl trimethoxy silane was the chemical that was used for increasing the bonding strength. It was diluted with 99 wt% of water and then the wire was submerged on the resulting solution for one hour, reproducing the same parameters that were observed in literature (Ghosh and Schiraldi, 2009).

After testing the specimens with chemically treated wire, the following curve was obtained through the tests (Figure 20):

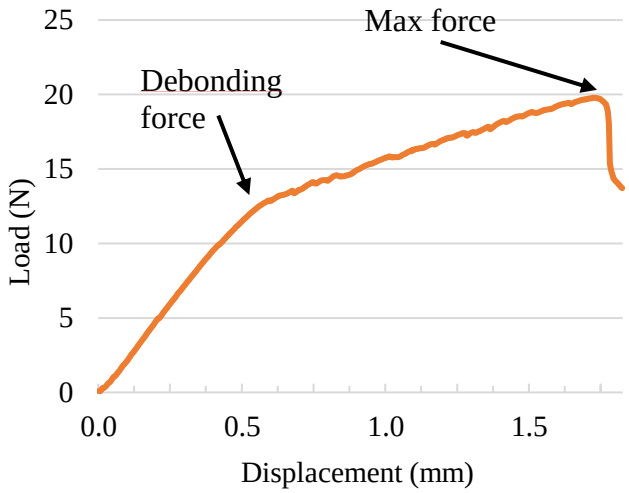

Figure 20: load vs extension curve of a chemically treated SMA wire embedded in TPU

This curve shows that the chemical treatment increased the debonding strength between the TPU and the Flexinol wire, but the maximum force was reduced from 40 to 20 N; thus, chemical treatment was discarded. The availability of a new flexible material developed in the W.M. Keck Center for 3D Innovation at the University of Texas at El Paso introduced the possibility of a switch in polymer material (Siqueiros *et al.*, 2016). This new material was first tested once, and the test produced promising results (Figure 21). The comparison of the adhesion

of the TPU and the ABS/SEBS materials with the SMA wire was the basis to change the material to the one with better adhesion as adhesion is important for the actuator application.

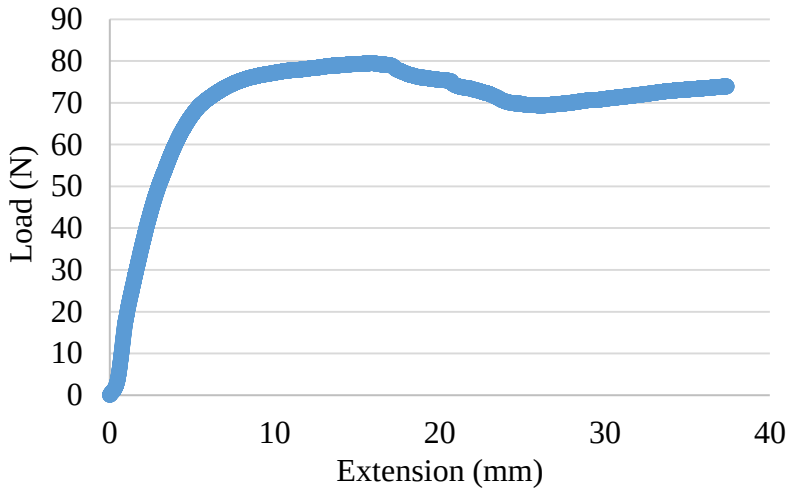

Figure 21: Load vs extension curve for Shape memory alloy embedded in ABS/SEBS blend of 90% SEBS.

The ABS/SEBS material is a blend developed in the W.M. Keck Center for 3D Innovation, containing 10% by weight of ABS and 90% by weight of SEBS. This blend follows the rule of mixtures, and this combination of ABS and SEBS results on a modulus of 15MPa. The adhesion tests that were performed showed that the bonding between the SMA wire and the ABS/SEBS polymer was strong (80N was recorded as maximum).

Figure 22 shows that the debonding of the wire from the ABS/SEBS blend was due to the deformation of the polymer rather than the force it was being pulled with. It is also observed how the tracks where the wire was embedded are being elongated without the wire in them. This drives the conclusion that it is this deformation of the polymer that induces debonding.

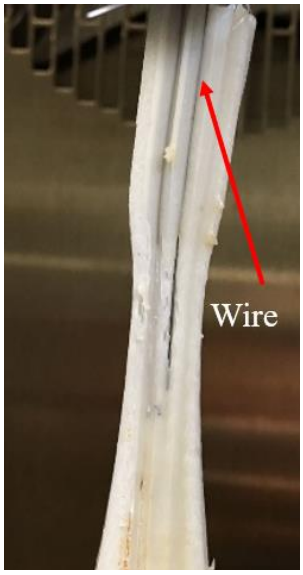

Figure 22: single fiber pullout test of SMA embedded on ABS/SEBS blend. Poisson's deformation is driving the debonding

A test for determining the ABS/SEBS material was conducted on five specimens. The curves obtained from this first formal test, although

they showed a failure at high extension throughout the 5 specimens, they showed failure was different from one another (Figure 23).

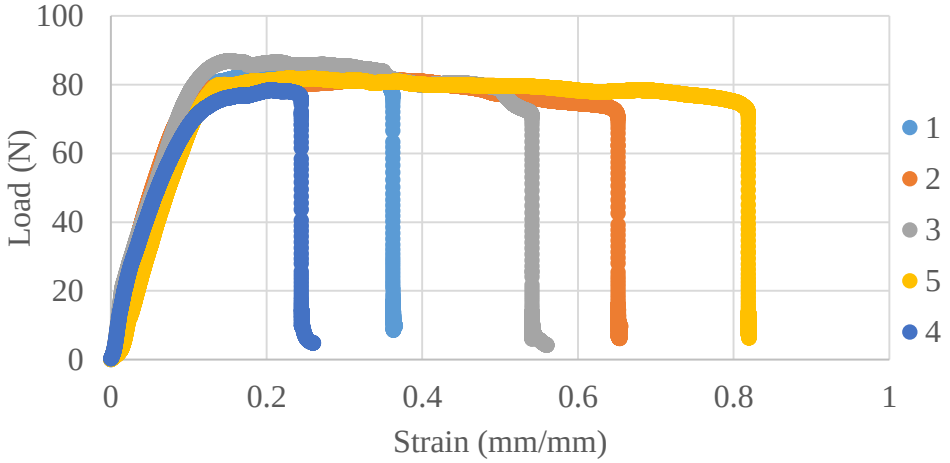

Figure 23: Load vs strain curves of 5 single fiber pullout tests performed on SMA wire embedded on the ABS/SEBS blend

After these curves were obtained, mechanical surface treatment of the wire was used to increase the bonding strength. Sanding of the surface area of the wire was performed, and SEM images were taken to determine if there was any difference on both surfaces, the mechanically treated and the untreated.

When looking at both wires under the SEM (Figure 24), it was observed that the surface of the wire had an oxide layer and that the mechanical treatment removed the oxide layer. Venables talks about how the presence of an oxide layer on the surface of the metal negatively affects the

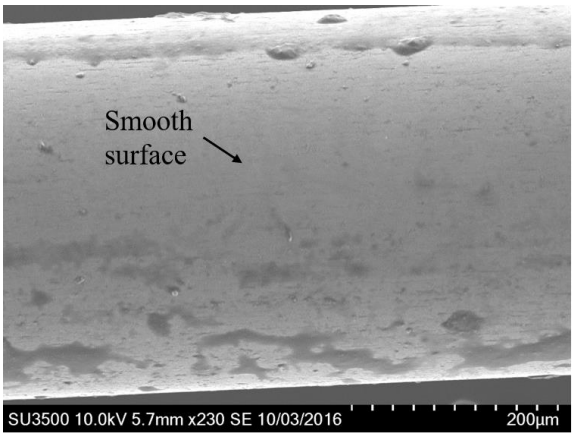

Original wire with no surface treatment

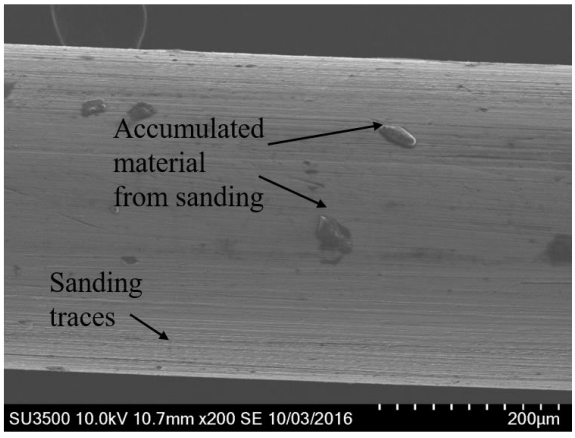

Sanded wire

Figure 24: SEM images of wire with no surface treatment and treated with sanding.

bonding between a polymer and a metal (Venables, 1984). For this reason, the oxide layer was removed. Also, Kim *et al*. talk about the increase of adhesion between polymer and metal with the introduction of micropatterned topography on the surface of the metal as the surface roughness plays an important role in adhesion (Kim *et al*., 2010). Not only was the oxide layer removed with this treatment, but the metal's potential bonding strength was increased by the traces that sanding left behind. This surface treatment was then tested with the same method and the following curve was obtained (Figure 25):

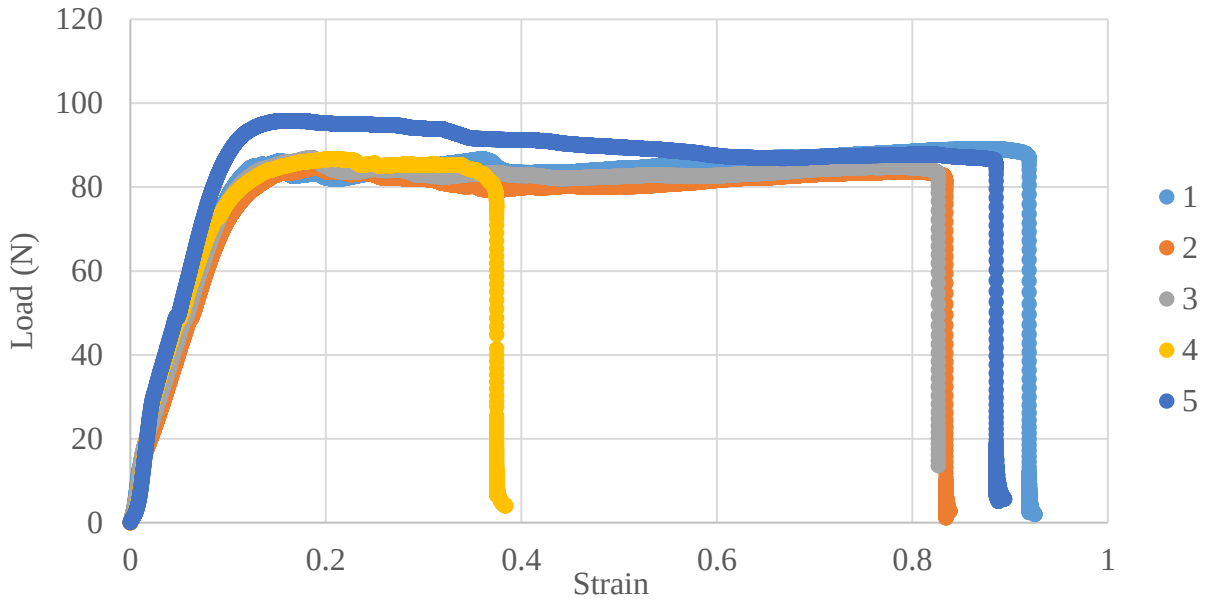

Figure 25: Load vs Strain curve for sanded SMA wire embedded in ABS/SEBS blend.

Within this curve, it is observed that the surface treatment had a positive effect on the bonding of the polymer to the wire. Most of the tests followed the same path until the end, showing that from non-treated and treated wires there is a difference, and it is found on the similarity of the results.

When a manufactured part for actuation testing was subjected to joule heating to determine actuation motion, plastic deformation was observed (Figure 26). After it was seen that the ABS/SEBS polymer would not work since it reconfigures after activation of the embedded wire, removing the recoverable motion, it was decided that materials had to be switched again.

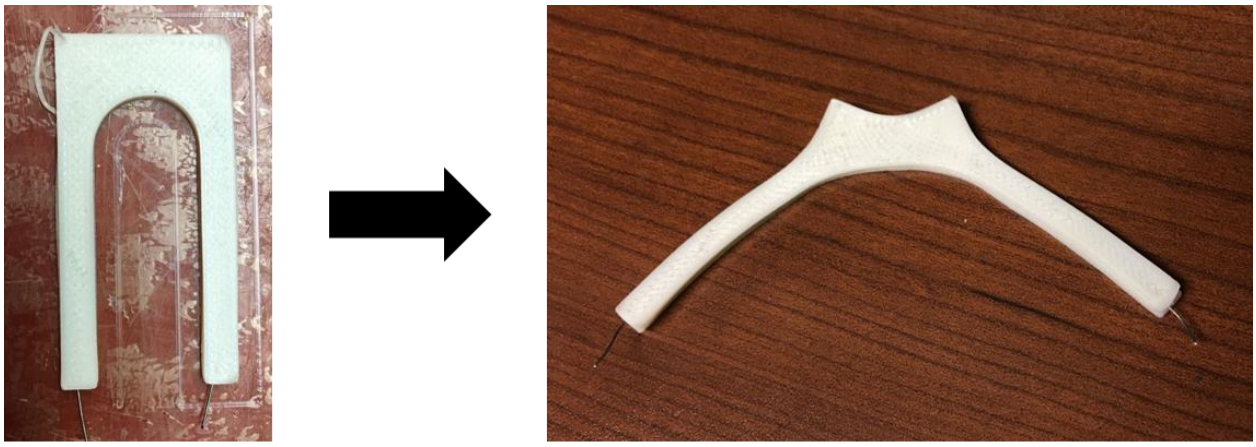

Figure 26: ABS/SEBS part before and after activation, no recovery after activation

Figure 27 shows the adhesion strength of 5 specimens made from PCTPE. These curves show an inconsistent trend of debonding; however, the debonding force ranges between ~15N and ~35N. All the drops observed in the graph show debonding of sections surrounding the wire. This means that the polymer was not debonding entirely from the wire. Instead, bonding was breaking on sections of the embedded interface.

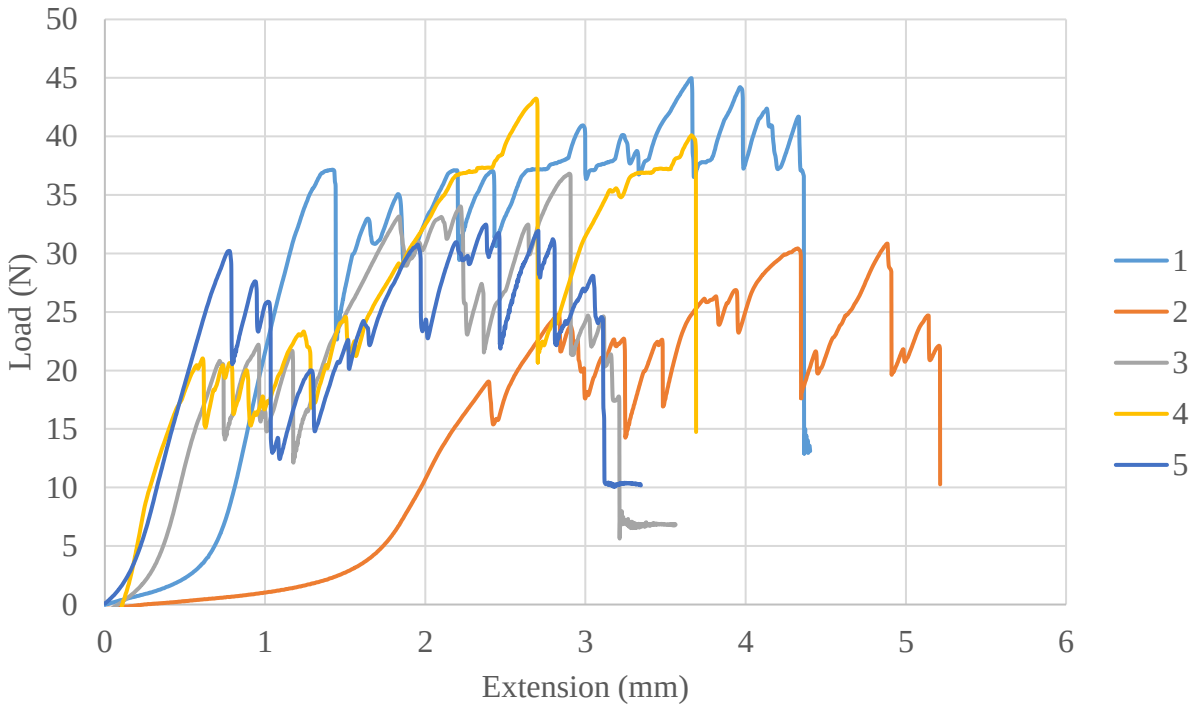

Figure 27: Load vs extension curve of PCTPE single fiber pullout test

5.2 HEAT TRANSFER MODELING

The results that the testing provided to validate the thermal modeling of the actuator are shown in the current vs time graphs. Although the infrared camera readings do not show accurate temperature readings because the emissivity change is a function of temperature, it is possible to develop a visual temperature map that can represent, only visually, the motion and the heating of

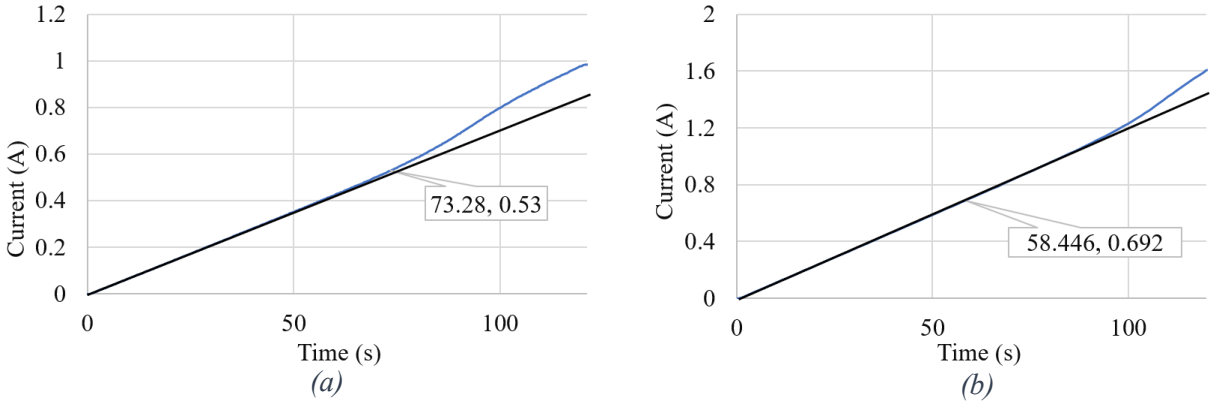

Figure 28: Current temperature curves for (a) wire in air and (b) wire in polymer. Straight black line on both graphs is to visually determine where the slope starts to change.

the wire.

The calculations that were made with the heat transfer model to reach 90°C, which is the activation temperature reported by the manufacturer, were 0.73A for the wire in air model and 0.59A for the wire in polymer. These are the desired current inputs to activate the wire.

The 9115 BK precision programmable power supply collected the current data of the tests and a change in the slope of the current curves was observed (Figure 28). This change in slope is due to the change of phase of the material that happens when the wire is activated. The change of phase also changes the electrical resistivity of the material. Figure 29 shows the IR imaging that was obtained through experiments. These images are for the wire prior to activation and after activation. The temperature of the wire can be observed as well as the motion that happened as a result of activation.

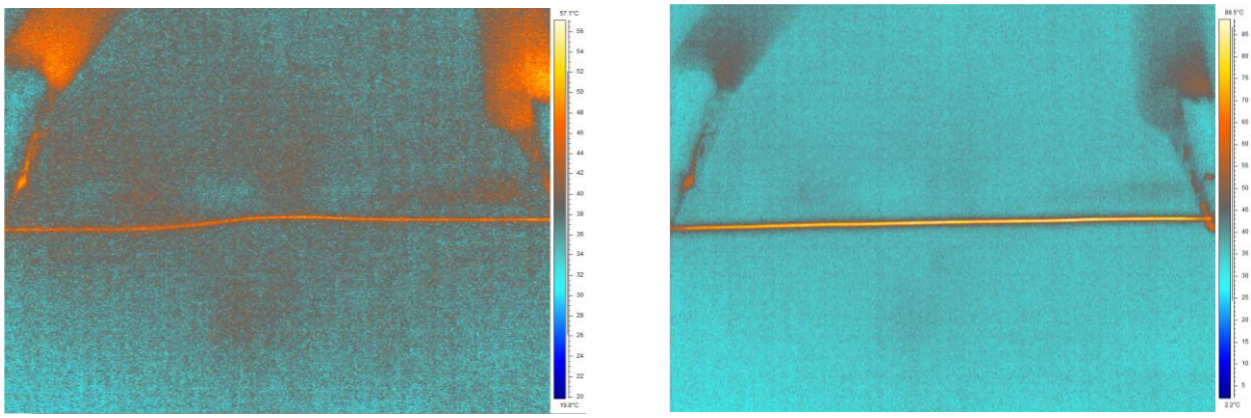

(a) (b)

Figure 29: IR imaging of the wire on air model. (a) Wire prior to activation at 45°C; (b) activated wire at 82.4°C

The wire moves due to a change of phase, the start of the change in slope observed in Figure 29 is where the wire undergoes the change of phase; thus, activation is happening. With this graph it is possible to validate the thermal modeling of the wire.

According to the strain vs temperature plot that the manufacturer provides (Figure 30), actuation initiates where strain is observed, in the area highlighted on the plot. The rapid change in slope means that activation is present and not precisely at 90°C to produce activation, which is the temperature that the manufacturer claims as activation temperature. With this information it is possible to deduce a temperature with the time vs current graphs. The current vs time graph of the

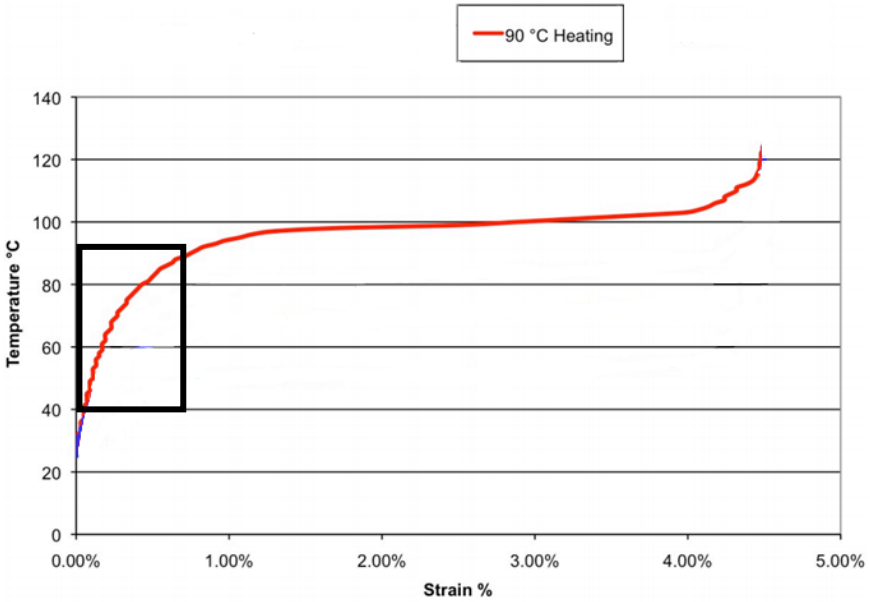

Figure 30: Temperature vs Strain curve of the SMA wire provided by the manufacturer (Dynalloy, 2018)

wire in air model shows a change of phase at about 0.53A. The calculations using this current resulted in about 60°C, which is in the range of temperatures where phase transformation happens, according to the plot in Figure 28. This shows the validity of the wire in air model.

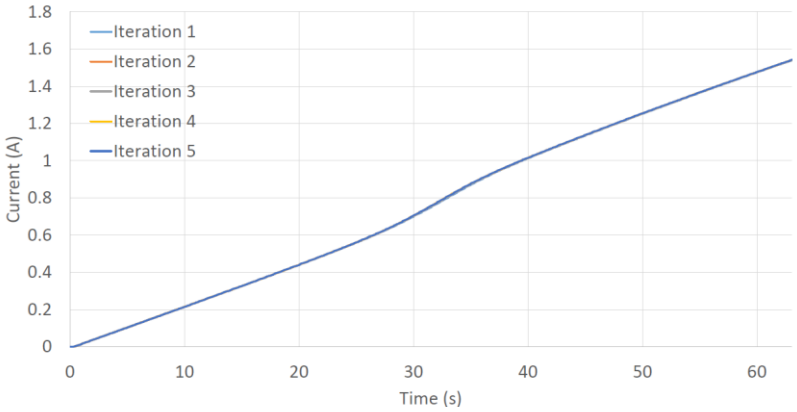

Figure 31: Current vs time plot for testing effects of repeated current induction on the wire.

Figure 31 contains the graphs that were produced by the repeated test ramps on the same wire. Five iterations were recorded on the same wire at 1.2V peak voltage. According to Figure 30, the wire was not affected by current passing through it as all the curves are overlayed on top of each other.

The wire in polymer model, on the other hand, could not be validated. The assumption that it was a steady state model could not replicate the experimental situation. On the current vs time graphs (Figure 28), the slope starts to change at about 0.7A. This means that the phase transformation starts when 0.7A are applied. However, the heat transfer model shows that at that current the temperature of the wire is already 117°C. Because of the strain vs temperature plot in Figure 30, it is possible to conclude that the model was not correct since the temperature for phase transformation to start should be around 60°C.

5.3 Repeatability Testing

For repeatability tests, periodic activation was implemented. This test was intended to validate the bending stress model and to provide data about the life of the actuator. First the rectangular cross-section part will be analyzed.

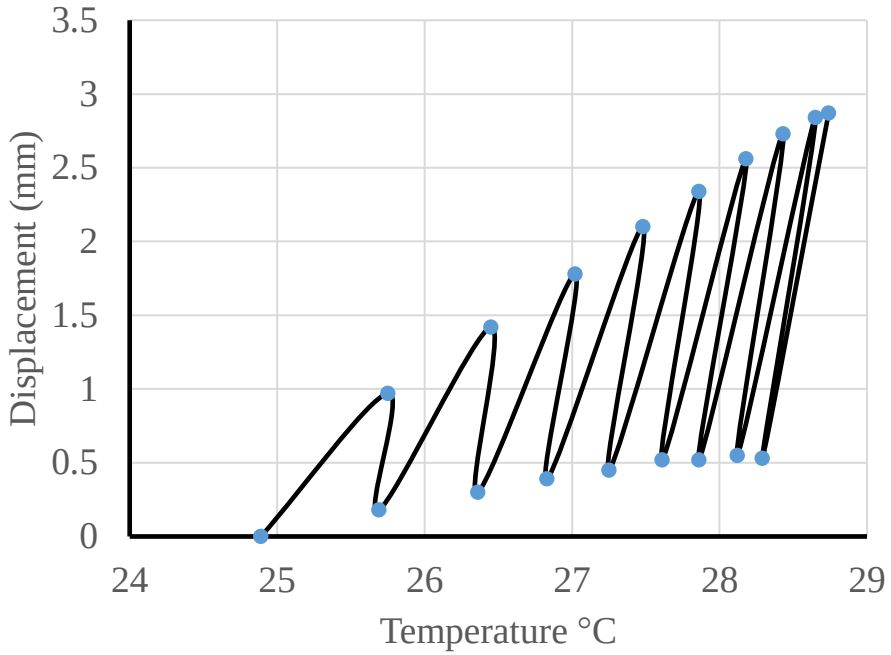

Figure 32: Displacement vs temperature curve for the activation cycling of actuator of 1 second current on and 10 seconds current off.

In the graph of Figure 32, it is observed that temperature constantly increases, leading to the conclusion that the polymer retains more heat than what it can dissipate in 10 seconds. However, the temperature increase helps in stabilization of the cycles of motion, as the temperature of the polymer increases the motion becomes more pronounced. The graph of Figure 32 also shows that displacement keeps increasing every cycle until it reaches about 2.75mm in total displacement. It also shows that the actuator is not recovering entirely (stopping at ~0.5mm). The increase of displacement and the lack of total recovery are effects of the temperature increase of the polymer. As the temperature of the polymer increases, it becomes more flexible and increases

the potential displacement every time it heats up; however, the higher temperature may not be letting the wire deactivate entirely.

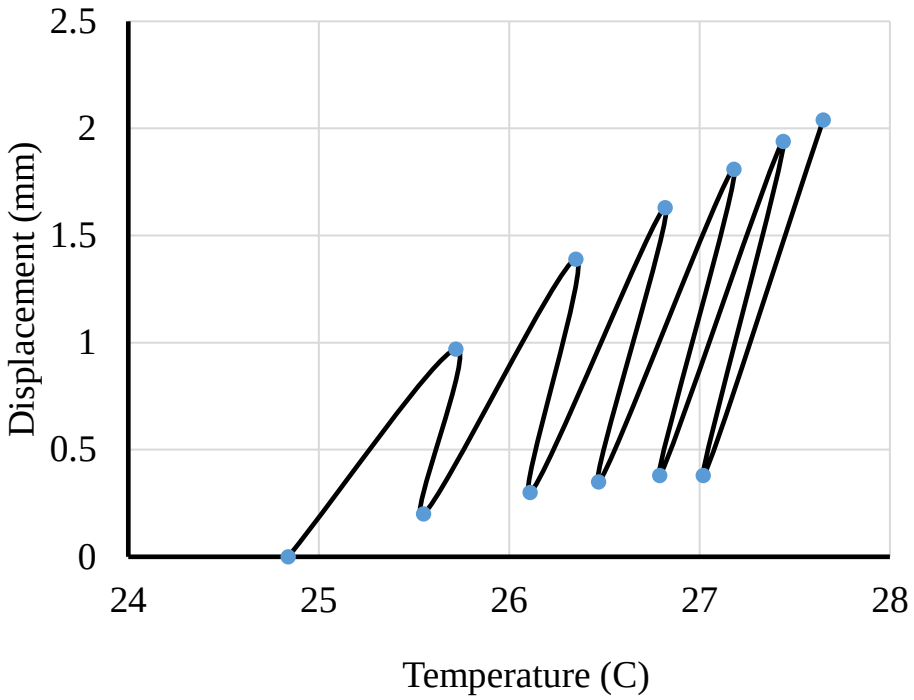

Figure 33: Displacement vs temperature curve for the activation cycling of actuator of 1 second current on and 15 seconds current off.

Figure 33 shows the results for the cyclical tests of 15 sec intervals. This graph shows that longer cooling times do not affect the displacement of the part, temperature decreases less than 1°C for 5 sec more of cool down time. Comparing the displacements between Figure 32 and 33, it was observed that more cooldown time. Although several more cycles are needed to reach steady state, it is expected to stay at between 28°C and 29°C, and the displacement will be 2.4 mm for every cycle with 10 seconds of cooldown time.

With the information gathered, it is possible to conclude that longer cooling cycles do not benefit the cyclical actuation. The higher temperature retained by the polymer increases the mobility of the part. Another test was made to corroborate the conclusion that consisted of cycling around 5 sec and it resulted in displacement above 3.25 mm, which is above the range of the

measuring equipment. This indicates that if the temperature of the actuator when it is not activated is increased, mores displacement will be present.

The cycle length does not affect the cyclical actuation. The periodic actuation reaches steady state when the temperature ceased to increase and when the displacement value is similar for several cycles, as shown in Figure 32. With every cycle the part heats up more and, as these actuators are temperature dependent, the start position of each cycle will continuously increase until heating reaches steady state.

The cylindrical specimen had a completely different behavior. The manufacturing of a 2 mm diameter cylinder with the Lulzbot TAZ 6 3D Printer was difficult due to the part being 2 mm in height. Embedding the wire onto the 2 mm surface had complications because of the small surface area where embedding had to happen and the surface roughness of this same area. Only one specimen was fully fabricated, and the reliability of this specimen could have been compromised because of the difficulty of manufacturing.

With the cylindrical specimen no motion was recorded when it was subjected to current. After it was determined that no motion was recorded, more current was induced on the wire with no success. This leads to the conclusion that the specimen fabricated was not reliable enough for testing.

CHAPTER 6: CONCLUSION AND FUTURE RECOMMENDATIONS

6.1 CONCLUSION

A method for creating actuators using additive manufacturing and wire embedding was developed. This method consisted of a heat transfer analysis and a bending stress analysis that would guide the design of actuator parts with the available properties of the materials used. Through experimentation and analysis of the properties of the polymers, it was possible to determine the requirements that this application demands.

It was determined that steady state assumptions do not work for heat transfer modeling because of the lack of similarity between the real case scenario and the model. The heat transfer model that was developed for wire in polymer did not show the expected validation quantities and thus could not be used for determining a current.

The bending stress analysis was determined to work for the rectangular cross-section model but for the circular, it was not possible to be validated due to technical limitations. The motion of the actuator with the rectangular cross-section was tested to be repeatable so an actuator could be created with this cross-sectional shape with the dimensions specified. Although repeatable motion was observed, the force of the actuator remains to be tested to suit the application's demands.

6.2 FUTURE WORK

Future work should include a transient heat transfer model with heat generation. This is to better determine the current needed to activate the wire inside the actuator. Also, it is important to revisit the assumptions for the bending stress model with the circular cross-sectional area for determining the minimum diameter needed for this type of actuation. Another path this research should pursue is the introduction of several wires to increase the actuation force that moves the actuator and to revisit the automatic embedding mechanisms for a systematical method for deposition of the wire. By pursuing this path, functional actuators can be created by additive manufacturing and wire embedding altogether.

REFERENCES

Aguilera E., Ramos J., Espalin D., Cedillos F., Muse D., Wicker R. et al. 3D printing of electro mechanical systems. In: 25th annual international solid freeform fabrication symposium. 2013. p. 950–61.

Ambriz, S., Coronel, J., Zinniel, B., Schloesser, R., Kim, C. Y., Perez, M., . . . Wicker, R. B. (2017). Material handling and registration for an additive manufacturing-based hybrid system. Journal of Manufacturing Systems, 45, 17-27. doi:10.1016/j.jmsy.2017.07.003

ASTM Standard F2792-12a. 2012. "Standard Terminology for Additive Manufacturing Technologies". ASTM International, West Conshohocken, PA.

Bailey, C., Aguilera, E., Espalin, D. Motta, J. F., Fernandez, A., Perez, M. A., Dibiasio, C., Pyputniewicz, D., MacDonald, E., Wicker, Ryan B. (2017). Augmenting Computer-Aided Design Software With Multi-Functional Capabilities to Automate Multi-Process Additive Manufacturing. in IEEE Access, 6, 1985-1994. doi: 10.1109/ACCESS.2017.2781249

Behl, M., & Lendlein, A. (2007). Shape-memory polymers. Materials Today, 10(4), 20-28. doi:Doi 10.1016/S1369-7021(07)70047-0

Bourell, D. L., Rosen, D. W., & Leu, M. C. (2014). The Roadmap for Additive Manufacturing and Its Impact. 3d Printing and Additive Manufacturing, 1(1), 6-9. doi:10.1089/3dp.2013.0002

Budynas, R. G., Nisbett, J. K., & Shigley, J. E. (2015). Shigley's mechanical engineering design (Tenth edition. ed.). New York, NY: McGraw-Hill Education.

Çengel, Y. A., & Ghajar, A. J. (2015). Heat and mass transfer: fundamentals & applications (Fifth edition. ed.). New York, N.Y.: McGraw-Hill.

Coronel, J. L., Fehr, K. H., Kelly, D. D., Espalin, D., & Wicker, R. B. (2017). Increasing component functionality via multi-process additive manufacturing. Micro- and Nanotechnology Sensors, Systems, and Applications Ix, 10194. doi:Unsp 101941f10.1117/12.2263257

da Silva, T. C., Sa, M. V. C., da Silva, E. P., & da Silva, F. C. (2016). Emissivity Measurements on Shape Memory Alloys. 13th Quantitative Infrared Thermography Conference, 172-179. doi:10.21611/qirt.2016.018

DiFrancia, C., Ward, T. C., & Claus, R. O. (1996). The single-fibre pull-out test .1. Review and interpretation. Composites Part a-Applied Science and Manufacturing, 27(8), 597-612. doi:Doi 10.1016/1359-835x(95)00069-E

Dynalloy Inc., 2018, 1070 Commercial Street, Suite No. 110, San Jose, California 95112. Website: www.dynalloy.com

Eceiza, A., Martin, M. D., de la Caba, K., Kortaberria, G., Gabilondo, N., Corcuera, M. A., & Mondragon, I. (2008). Thermoplastic polyurethane elastomers based on polycarbonate diols with different soft segment molecular weight and chemical structure: Mechanical and thermal properties. Polymer Engineering and Science, 48(2), 297-306. doi:10.1002/pen.20905

Espalin, D., Muse, D. W., MacDonald, E., & Wicker, R. B. (2014). 3D Printing multifunctionality: structures with electronics. International Journal of Advanced Manufacturing Technology, 72(5-8), 963-978. doi:10.1007/s00170-014-5717-7

Espalin, D., Ramirez, J. A., Medina, F., & Wicker, R. (2014). Multi-material, multi-technology FDM: exploring build process variations. Rapid Prototyping Journal, 20(3), 236-244. doi:10.1108/Rpj-12-2012-0112

Feng, H. B., Lu, X. Y., Wang, W. Y., Kang, N. G., & Mays, J. W. (2017). Block Copolymers: Synthesis, Self-Assembly, and Applications. Polymers, 9(10). doi:ARTN 49410.3390/polym9100494

Gall, K., Yakacki, C. M., Liu, Y. P., Shandas, R., Willett, N., & Anseth, K. S. (2005). Thermomechanics of the shape memory effect in polymers for biomedical applications. Journal of Biomedical Materials Research Part A, 73a(3), 339-348. doi:10.1002/jbm.a.30296

Ghosh, A., & Schiraldi, D. A. (2009). Improving Interfacial Adhesion Between Thermoplastic Polyurethane and Copper Foil Using Amino Carboxylic Acids. Journal of Applied Polymer Science, 112(3), 1738-1744. doi:10.1002/app.29787

Grace, R. (2016). Additive manufacturing faces challenges as it grows: but new technologies may open up options for designers for producing 3-D-printed parts better & faster. Plastics Engineering, 72(2), 8+. Retrieved from http://0-link.galegroup.com.lib.utep.edu/apps/doc/A443654676/SCIC?u=txshracd2603&sid=SCIC&xid=21b275d1

Bual, G. S., Kumar, P. (2014). Methods to Improve Surface Finish of Parts Produced by Fused Deposition Modeling. Manufacturing Science and Technology, 2, 51 - 55. doi:10.13189/mst.2014.020301.

Hossain, M. S., Espalin, D., Ramos, J., Perez, M., & Wicker, R. (2014). Improved Mechanical Properties of Fused Deposition Modeling-Manufactured Parts Through Build Parameter Modifications. Journal of Manufacturing Science and Engineering-Transactions of the Asme, 136(6). doi:Artn 06100210.1115/1.4028538

Ilgevicius, A. (2004). Analytical and numerical analysis and simulation of heat transfer in electrical conductors and fuses. Universität der Bundeswehr München.

Kim, C., Espalin, D., Cuaron, A., Perez, M. A., Lee, M., MacDonald, E., & Wicker, R. B. (2015). Cooperative Tool Path Planning for Wire Embedding on Additively Manufactured Curved Surfaces Using Robot Kinematics. Journal of Mechanisms and Robotics-Transactions of the Asme, 7(2). doi:Artn 02100310.1115/1.4029473

Kim, W. S., Yun, I. H., Lee, J. J., & Jung, H. T. (2010). Evaluation of mechanical interlock effect on adhesion strength of polymer-metal interfaces using micro-patterned surface topography. International Journal of Adhesion and Adhesives, 30(6), 408-417. doi:10.1016/j.ijadhadh.2010.05.004

Lagoudas, D. C. (2008). Shape memory alloys: modeling and engineering applications. New York ; London: Springer.

MacDonald, E., Espalin, D., Doyle, D., Munoz, J., Ambriz, S., Coronel, J., . . . Wicker, R. (2018). Fabricating patch antennas within complex dielectric structures through multi-process 3D printing. Journal of Manufacturing Processes, 34, 197-203. doi:10.1016/j.jmapro.2018.05.013

MacDonald, E., Salas, R., Espalin, D., Perez, M., Aguilera, E., Muse, D., & Wicker, R. B. (2014). 3D Printing for the Rapid Prototyping of Structural Electronics. IEEE Access, 2, 234-242. doi:10.1109/Access.2014.2311810

Meo, M., Marulo, F., Guida, M., & Russo, S. (2013). Shape memory alloy hybrid composites for improved impact properties for aeronautical applications. Composite Structures, 95, 756-766. doi:10.1016/j.compstruct.2012.08.011

Qiu, J. S., Lim, X. N., & Yang, E. H. (2016). Fatigue-induced deterioration of the interface between micro-polyvinyl alcohol (PVA) fiber and cement matrix. Cement and Concrete Research, 90, 127-136. doi:10.1016/j.cemconres.2016.08.021

Rediniotis, O. K., Wilson, L. N., Lagoudas, D. C., & Khan, M. M. (2002). Development of a shape-memory-alloy actuated biomimetic hydrofoil. Journal of Intelligent Material Systems and Structures, 13(1), 35-49. doi:10.1106/104538902028534

Rogers C. A., (1998). Active vibration and structural acoustic control of shape memory alloy hybrid composites: Experimental results. The Journal of the Acoustical Society of America, 88(6), 2803-2811. doi: 10.1121/1.399683

Shemelya, C., Banuelos-Chacon, L., Melendez, A., Kief, C., Espalin, D., Wicker, R., . . . MacDonald, E. (2015). Multi-functional 3D Printed and Embedded Sensors for Satellite Qualification Structures. 2015 IEEE Sensors, 1422-1425.

Shemelya, C., Cedillos, F., Aguilera, E., Espalin, D., Muse, D., Wicker, R., & MacDonald, E. (2015). Encapsulated Copper Wire and Copper Mesh Capacitive Sensing for 3-D Printing Applications. IEEE Sensors Journal, 15(2), 1280-1286. doi:10.1109/Jsen.2014.2356973

Shemelya, C., Zemba, M., Liang, M., Yu, X. J., Espalin, D., Wicker, R., . . . MacDonald, E. (2016). Multi-layer archimedean spiral antenna fabricated using polymer extrusion 3D printing. Microwave and Optical Technology Letters, 58(7), 1662-1666. doi:10.1002/mop.29881

Shemelya, C. M., Zemba, M., Liang, M., Espalin, D., Kief, C., Xin, H., . . . MacDonald, E. W. (2015). 3D PRINTING MULTI-FUNCTIONALITY: Embedded RF Antennas and Components. 2015 9th European Conference on Antennas and Propagation (EuCAP).

Singh, R. (2010). Three Dimensional Printing for Casting Applications: A State of Art Review and Future Perspectives. Advances in Materials and Processing Technologies, Pts 1 and 2, 83-86, 342-349. doi:10.4028/www.scientific.net/AMR.83-86.342

Siqueiros, J. G., Schnittker, K., & Roberson, D. A. (2016). ABS-maleated SEBS blend as a 3D printable material. Virtual and Physical Prototyping, 11(2), 123-131. doi:10.1080/17452759.2016.1175045

Spontak, R. J., & Patel, N. P. (2000). Thermoplastic elastomers: fundamentals and applications. Current Opinion in Colloid & Interface Science, 5(5-6), 334-341.

Takaku, A., & Arridge, R. G. C. (1973). Effect of Interfacial Radial and Shear-Stress on Fiber Pull-out in Composite-Materials. Journal of Physics D-Applied Physics, 6(17), 2038-2047. doi:Doi 10.1088/0022-3727/6/17/310

Venables, J. D. (1984). Adhesion and Durability of Metal Polymer Bonds. Journal of Materials Science, 19(8), 2431-2453. doi:Doi 10.1007/Bf00550796

Voit, W., Ware, T., Dasari, R. R., Smith, P., Danz, L., Simon, D., . . . Gall, K. (2010). High-Strain Shape-Memory Polymers. Advanced Functional Materials, 20(1), 162-171. doi:10.1002/adfm.200901409

Yener, Y., Kakaç, S., & Kakaç, S. (2008). Heat conduction (4th ed.). New York: Taylor & Francis.

VITA

Alfonso Fernandez was born on March 11, 1993 and is the son of Mr. Alfonso Fernandez (1955-2013) and Mrs. Maria R. Dominguez. Alfonso obtained a high school diploma on May 2011 from ITESM in Ciudad Juarez. He received a Bachelor of Science Degree in Mechanical Engineering from the University of Texas at El Paso in 2015. While pursuing a graduate degree, Alfonso helped college students with classes by tutoring. In 2015, he received the "Best business plan" award at the 2015 Paso Del Norte Venture Competition along with the "Best presentation" award.

afernandez16@miners.utep.edu